Ionics (2023) 29:9–32
https://doi.org/10.1007/s11581-022-04774-2

REVIEW

Advances in nonprecious metal catalysts for efficient water oxidation in alkaline media

Sheng Chen[1] · Yihan Wang[1] · Zhijun Wang[2] · Kun Zhang[1]

Received: 24 April 2022 / Revised: 24 August 2022 / Accepted: 22 September 2022 / Published online: 19 October 2022

Abstract

Fossil fuels are facing various challenges, such as global warming and depletion of fossil energy sources. Fortunately, hydrogen energy can be a green energy source for sustainable development. Hydrogen production from electrolytic water is one of the most efficient methods in the hydrogen energy industry; however, the realization of an efficient electrochemical oxygen evolution reaction (OER) is the key to hydrogen production from electrolytic water. As a result, developing noble metal-free electrocatalysts with high activity and alkaline stability is critical. This article gives a focused evaluation of the most recent highly active oxygen evolution catalysts in this new research field. The mechanism of the OER catalyst in an alkaline environment is discussed first, followed by the fundamental needs of catalysts for the oxygen evolution process. Then, contemporary researchers' design alternatives for enhancing OER active materials are explored, as well as new developments and discoveries of current advanced noble metal-free active materials. Finally, the problems and future prospects for developing efficient catalyst systems for industrial applications are discussed. Future research directions are also pointed out for the preparation of resource-rich emerging nonprecious metal OER electrocatalysts in alkaline environments.

Keywords Electrocatalysts · Precious-metal-free catalysts · Hydrogen production · Water oxidation · Alkaline media

Introduction

Nowadays, fossil energy and the global environmental crisis necessitate the exploration and developing of alternative energy sources and economic storage solutions, such as solar, wind and hydrogen energy [1]. Among various solutions, splitting of water to hydrogen energy has aroused enthusiastic attention due to its high efficiency and environmental friendliness [2–4]. Water splitting process consists of two half-reactions, the oxygen evolution reaction (OER, $2H_2O \rightarrow O_2 + 4H^+ + 4e^-$) and the hydrogen evolution reaction (HER, $2H^+ + 2e^- \rightarrow H_2$). Both OER and HER are kinetic multistep processes that require additional energy to overcome the activation barrier. The OER is a four-electron transfer mechanism, and requires larger overpotential than HER to deliver an appreciable current, which limits the entire water decomposition (OWS) process [5, 6]. As a result, it is critical to investigate highly catalytically active oxygen evolution materials and to assess electrocatalyst performance by overpotential at a current density of 10 mA cm^{-2}.

Electrochemical hydrolysis is often carried out in alkaline or acidic electrolytes. Alkali conditions result in quicker ion transport between the cathode and anode, as well as faster hydrogen generation via reaction kinetics. Noble metal catalysts such as RuO_2, Pt, IrO_2, and noble metal-based compounds [7–9] are usually used as the benchmark OER catalysts in alkaline media, but the high cost and poor stability seriously limit their wide applications. Therefore, substantial efforts have been devoted to seeking cost-effective, abundant, and efficient OER catalysts OER. Most nonprecious metal reactive compounds, such as cobalt-based sulfides and selenide films, work well in neutral to alkaline environments [10]. Interestingly, several transition metal-based materials have approached or even surpassed the electrocatalytic performance of precious metals in the development of sophisticated nonprecious metal materials to

✉ Yihan Wang
yhwang027@scu.edu.cn

[1] Key Laboratory of Radiation Physics and Technology of Ministry of Education, Institute of Nuclear Science and Technology, Sichuan University, Chengdu 610064, China

[2] Institute for Advanced Study, Chengdu University, Chengdu 610106, China

maximize the catalytic performance of their OER or bifunctional catalysts [11, 12]. For example, some Ni-, Co-, and Fe-based nanomaterials have been used as super catalysts for OER [13–15]. Layered double hydroxides (LDHs) of Ni–Fe-based oxides and (oxygen) hydroxides are considered as materials with high catalytic activity potential for OER [16–18]. In addition, carbon-based materials with metallic properties, nonprecious nitrogen compounds, sulfides, and metal–organic framework (MOF) derivatives exhibit excellent OER performance under alkaline conditions [19–21]. Thus far, OER catalysts with refined structure and morphologies (nanosheets, nanorods, nanoparticles) have been proven practical. In addition, designing electronic structure reconstruction of catalysts (defects, vacancies) or doping elements can effectively improve the catalytic activity of catalysts. On this basis, potential catalyst design and performance optimization methodologies for guiding the synthesis of alkali-resistant materials with high catalytic activity and stability may be created [22–25].

The current state of research on oxygen-resistant catalytic materials in alkali is reviewed in this paper. The fundamental concepts of OER are discussed first, including the reaction process, physicochemical property requirements, and design suggestions for oxygen precipitation catalysts in bases. This is critical for comprehending the relevant catalytic activity. Then, case studies of nonprecious metal oxides, MOFs, nitrides, sulfides, hydroxides, and the newly developing high-entropy materials catalysis are shown to illustrate the benefits of various types of compounds in the field of OER. Finally, major difficulties confronting the development of noble metal-free electrocatalysts for OER in alkaline solutions are highlighted, presenting insight into future research. We expect that the information presented here will assist to pave the way for future research on noble metal-free electrocatalysts for OER in alkaline solutions.

OER catalyst in alkaline environment

Reaction mechanism

Figure 1 [6] depicts a widely accepted mechanism for the oxygen evolution reaction at the anode electrode, and it was discovered that its intermediates are identical under alkaline or acidic conditions. Most of the mechanisms proposed by researchers involve the same intermediates, such as M-OH, M–O, and M-OOH, where M denotes the material surface metal. As shown in Fig. 1, one is a green route that forms O_2 in direct succession via 2 M–O, and the other involves the generation of an M-OOH intermediate, which subsequently decays to O_2 (the black route in Fig. 1). Despite some differences, the bonding (M–O) between the OER intermediates

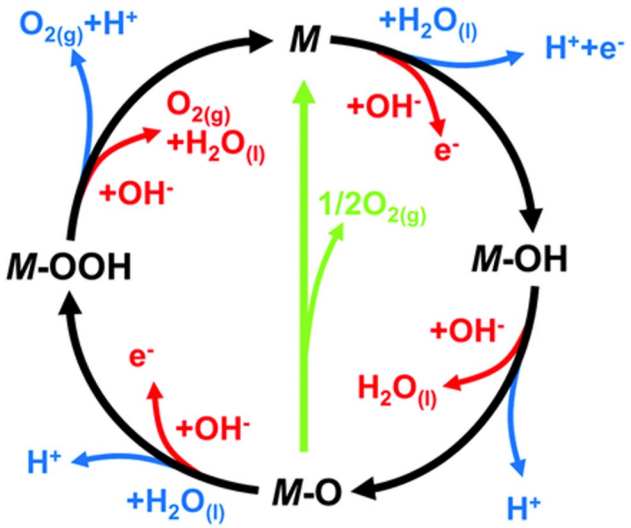

Fig. 1 The OER mechanism for acid (blue line) and alkaline (red line) conditions. The black line indicates that the oxygen evolution involves the formation of a peroxide (M–OOH) intermediate (black line) while another route for direct reaction of two adjacent oxo (M–O) intermediates (green) to produce oxygen is possible as well. Reproduced with permission from Ref. [6]

(M-OH, M–O, M-OOH) is generally considered to be critical to the overall electrocatalytic performance.

Under alkaline conditions, the OER process involves the electron transfer processes of multiple intermediates, as described by the following equations [26]:

$$OH^- + * \rightarrow HO^* + e \quad (1)$$

$$HO^* + OH^- \rightarrow O^* + H_2O + e \quad (2)$$

$$O^* + OH^- \rightarrow HOO^* + e \quad (3)$$

$$HOO^* + OH^- \rightarrow * + O_2 + H_2O + e \quad (4)$$

where * represents the active spot on the catalyst's surface. In the first step, OH^- is directly adsorbed on the catalyst surface in alkaline medium to form intermediate product OH*; in the second step, OH^- combines with intermediate product OH* to form H_2O molecule and substable intermediate O*; in the third step, O* combines with OH^- directly to form HOO*; and finally, HOO* combines with OH– to release O_2.

It is demonstrated that the OER process is a multistep single electron transfer process from the above reaction mechanism. The intermediates O* and O* in OER cannot be directly combined to generate O_2, and its generation directly depends to a large extent on the activation energy between the OER intermediate and the catalyst surface. So, each intermediate is produced with a certain amount of energy

from outside. As a result, we aim to find the optimum catalyst with strong OER activity that can give both HO∗ and HOO∗ in the reaction process. However, the simultaneous binding of catalysts to HO∗ and HOO∗ is a difficult topic of current study since it is difficult to accomplish merely by regulating the catalytic surface [27]. The activity of RuO_2 is theoretically anticipated based on the binding energy of the chemical intermediate and the catalyst, and it is near the top of the volcano (Fig. 2a). Besides, the computed results correspond with the actual data (10 mA cm^{-2} overpotential) (Fig. 2b), demonstrating the rationality and universality of the model. Clearly, thermochemical analysis based on density generalized theory (DFT) calculations allow the prediction of the trend of OER catalytic activity and aid in the creation of new sophisticated OER catalysts [28].

Design strategy of nanostructured electrocatalysts

We can create nonprecious metal compounds by selecting elements from the periodic table that can quickly evolve oxygen in alkaline high oxidation potential situations (carbon, nitrogen, phosphorus, sulfur, hydrogen, oxygen, cobalt, manganese, lead, iron, titanium, tin, nickel, antimony) in order to further improve the catalytic performance of the above compounds. In addition, another factor to consider is electrical conductivity, which plays an important role in electrocatalysis. The high conductivity ensures a fast electron transfer process, which can greatly improve energy conversion efficiency by reducing the overpotential caused by the catalyst–electrolyte and catalyst–electrode interfaces' Schottky barrier [29–31].

Therefore, we measure the conductivity of the catalyst to see if the conductivity affects the measured OER activity. For the powdery solid catalyst, conductivity can be measured in dry pressed particles or powder compression chambers [32]. However, considering that many catalysts recombine dynamically under OER conditions, out-of-field conductivity measurements are insufficient. In situ measurements of conductivity at electrolyte and OER-associated potentials can be made using interdigitated array microelectrodes (IDAs). Steady-state in situ film conductivity measurements are made by applying a constant potential offset of 10 mV between two IDA working electrodes (WE1 and WE2) while WE1 is held constant relative to the reference electrode for 2–5 min until the measurement current stabilizes. In this dual working electrode conductivity experiment, the current measured at each working electrode can be described as the sum of the Faraday and transmembrane conductive components:

$$I_{WE1} = I_{OER1} + I_{cat1} + I_{cond} \tag{5}$$

$$I_{WE2} = I_{OER2} + I_{cat2} - I_{cond} \tag{6}$$

where I_{WE1} and I_{WE2} are the total current measured at each working electrode, I_{OER} is the current from OER, I_{cat} is the current from catalyst oxidation, and I_{cond} is the transmembrane conductivity current. Because the working electrode is symmetric, $I_{OER1} \approx I_{OER2}$ and $I_{cat1} \approx I_{cat2}$. Therefore, $I_{WE1} - I_{WE2} \approx 2I_{cond}$. The effective catalyst film conductivity σ is estimated by the formula below:

$$\sigma_{eff} = \frac{I_{cond} w}{Nld\Delta V} \tag{7}$$

where w is the IDA gap spacing, N is the number of electrodes (here $N = 130$), l is the length of each electrode, d is the thickness of the film, and ΔV is the voltage offset between WE1 and WE2 (here $\Delta V = 10$ mV) [33].

In the next sections, we will discuss several strategies, including chemical doping, defect (vacancy) engineering, phase engineering, facet engineering, and structural engineering, to improve OER catalytic performance (Fig. 3).

The OER always takes place on the surface of the electrode, and even if an inert material is employed as the

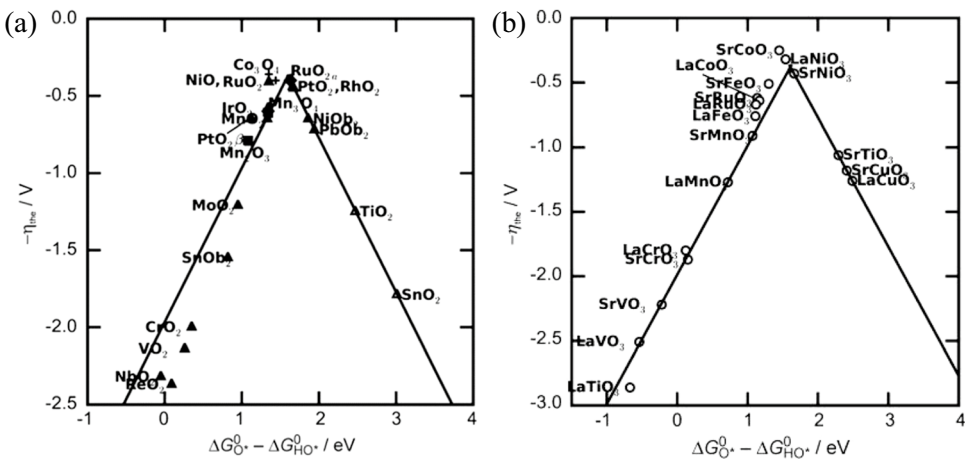

Fig. 2 Volcano-shaped activity plot of the OER for **a** oxides and **b** perovskites. The negative thermodynamically calculated overpotential was plotted against the difference between the energy states of *HO and *O, $\Delta G^0_{O^*} - \Delta G^0_{OH^*}$. Reproduced with permission from Ref. [27]

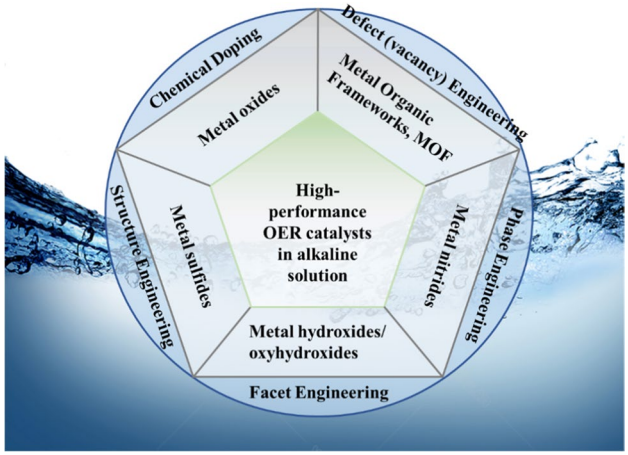

Fig. 3 Scheme showing the main physicochemical feature requirements and implementation approaches for a high-performance OER electrocatalyst in alkaline solution

anode, an oxide layer is always generated on the surface of the potential region where oxygen precipitates in the OER. However, the development of oxides on the anode always has an impact on the OER mechanism and the electrocatalytic activity of the catalyst. Fortunately, modifying the interfacial properties of the catalyst to obtain the superhydrophobic (hydrophilic) materials provides an efficient way [34]. On one hand, with bubbles highly deposited on the electrode materials' surface during the OER process, the electron transfer efficiency will be reduced. Superhydrophobic (superhydrophilic) materials, on the other hand, can reduce bubble stickiness and attachment time on the materials' surface, allowing for the quick release of OER-generated bubbles [35, 36]. Electrodeposition techniques, hydrothermal processes, and high-temperature vapor-phase growth have all been demonstrated to be useful in obtaining superhydrophobic (superhydrophobic) materials [37–39]. It is worth mentioning that achieving high roughness by adjusting the pore size and surface area of nanoarray-structured materials is a significant aspect of creating superhydrophobic (superhydrophobic) surfaces [40]. In addition, while being used, catalysts undergo surface reconfiguration, which could present another potential for catalytic materials. Therefore, surface pre-reconfiguration is a method for increasing the catalytic activity of catalysts. Although we do understand some aspects of catalyst surface regeneration, it is still unclear what function it serves. Zhao et al. [41] discovered that during low-voltage discharge, the catalyst creates new oxygen vacancies. These in situ created vacancies can enhance the surface electron configuration for intermediate adsorption, hence increasing reaction kinetics. In addition, as a result of the discharge process's accelerated mass transfer, there are more active sites. Wu et al. [42] found that defects on the catalyst surface are gradually disordered as the applied voltage increases, and when the voltage is high enough, oxygen is produced and other localized objects are generated.

The electrical structure of the material may be switched from normal semiconductor to metallic qualities by adding defects (vacancies), allowing the materials to acquire more electrons and achieve better electrocatalytic capabilities [43, 44]. The design of oxygen vacancies was shown to be beneficial in modulating the material's adsorption energy to water and obtaining the H adsorption minimum near 0 eV [45]. The defect (vacancy) design methods for materials are low-temperature plasma techniques, hydrothermal methods, etc. Among them, the low-temperature plasma technique is an efficient and controllable method to create vacancies in materials and improve their catalytic properties. This technique is able to change the electronic structure and produce more defects, thus increasing the active centers. It is important for us to study the mechanism of defect (vacancy) generation and its enhancement of the performance of electrochemistry.

A series of rare earth-rich transition metal-based materials (including oxides, sulfides, nitrides, borides, and phosphides) can be doped with heteroatoms by chemical doping [46–48], which are doped mainly to improve the electrochemical performance through energy-level hybridization between the dopant and the original catalyst. It has been found that chemical doping involves energy band engineering, d-band center, valence and charge redistribution of the active site, and optimization of the formation energy of the intermediates, which favor the precipitation of the decomposition gas of H_2O. Compared to metal doping, nonmetal doping would be more stable and effective and could better optimize the catalyst matrix to achieve hydrolysis [26, 49].

Modulation of the specific surface area [50, 51] and particle size [52] of the electrode is also a very effective scheme to obtain efficient oxygen evolution electrodes. Generally, by modulating the surface area and particle size of the material, small planar structures with more visible defects can be obtained, such as vacancies, edge positions, lattice defects, and other defects, which can provide more active sites for electrocatalysis in the materials we prepare [53]. Nanostructured materials with a high specific surface area can provide more active sites to contact during electrolysis of water compared to bulk materials with smooth surfaces. Furthermore, this can promote the adequate transportation of reactants and products. These properties are reflected in the high catalytic activity of the material [54]. After extensive research, researchers have prepared nanostructures with different shapes, such as nanopores, nanosheets, and nanowires [55]. Nanoporous materials and nanosheet structures are mainly shown to provide more active sites and ensure effective electron transport during the reaction. Nanotube structures facilitate electron and ion transport because of their one-dimensional (1D) structures, their tubular geometry

provides enough internal free space to accommodate large volume changes, and their large surface area maximizes the contact between the electrode and electrolyte [56].

The catalytic properties of catalysts with different crystal forms are also different [57]. For example, α-PbO_2 has smaller grain size and distortion, and β-PbO_2 has good corrosion resistance and conductivity [58]. When compared to the 2H phase, TMS in metal 1 T or metal monoclinic 1 T′ has superior charge transport capacity [44]. In experiments, the crystal structure of metal atoms is often modulated by tuning their chemical bonds [59], and the catalytic properties corresponding to different crystal structures are used to prepare excellent OER catalysts, promoting electrode kinetic electrocatalysts, increasing catalytic active sites, and improving corrosion resistance.

Various nonprecious metal electrocatalytic oxygen precipitation catalysts

Currently, research on low-cost catalyst materials is the focus of water electrolysis for hydrogen production. In this chapter, we primarily review the recent progress of OER nonprecious metal-based materials in alkaline media. Furthermore, composite compounds made of mixed metal carbides, borides, nitrides, sulfides, or phosphides were created to boost their effectiveness as catalysts. These composites not only outperform pure metals in terms of corrosion resistance, but also perform at a cheaper cost in terms of electrical conductivity and long-term stability. As a result, utilizing these materials as carriers or directly as electrocatalysts results in improved activity and stability. As indicated in

Table 1 The previously reported catalytic performance of nonprecious metal electrocatalysts for OER in alkaline conditions was compared

Catalyst/substrate	Key strategy	Electrolyte @298 K	Loading ($mg.cm^{-2}$)	η for OER (mV @ $mA.cm^{-2}$)	Tafel slope ($mV.dec^{-1}$)	Ref
Co_3O_4/N-rmGO	Metal oxides	1 M KOH	0.24	154 @ 10	67	[60]
Co_3O_4		0.1 M KOH	\	153 @ 10	68	[61]
P-Co_3O_4		1 M KOH	\	280 @ 10	51.6	[49]
O-Co_3O_4		1 M KOH	\	145 @ 10	49.1	[62]
Ni/NiO		1 M KOH	\	382 @ 100	103	[63]
NS-MnO_2		1 M KOH	\	138 @ 10	40	[52]
WO_3/CC		1 M KOH		280 @ 10	82	[64]
$BiFeO_3$		1 M NaOH	\	123 @ 0.16	\	[65]
$GaFeO_3$		0.1 M KOH	\	390 @ 10	\	[58]
$La_{0.5}Sr_{0.5}CoO_{3-x}$		0.1 M KOH	\	148 @ start	\	[59]
NF@NC-$CoFe_2O_4$/C NRAs	MOF-derived carbon-based materials	1 M KOH	1.03	145 @ 10	45	[66]
$CoFe_2O_4$/C@CP		1 M KOH	\	150 @ 10	70	[67]
Fe_2Ni MOF/NF		1 M KOH	\	222 @ 10	42.39	[68]
Ti_3C_2Tx–CoBDC		0.1 M KOH	0.21	164 @ 10	48.2	[69]
Fe/$Ni_{2.4}$/$Mn_{0.4}$-MIL-53		1 M KOH	0.51	236 @ 20	52.2	[70]
$Co_{2.36}Fe_{0.19}Ni_{0.45}$-btca		1 M KOH	\	292 @ 10	72.6	[71]
Ni-UMOFNs		1 M KOH	0.2	250 @ 10	103	[72]
Ni-MOF@Fe-MOF		1 M KOH	0.2	265 @ 10	82	[73]
CoN/NF	Metal nitrides	1 M KOH	\	290 @ 10	70	[74]
Nifoam@Ni–$Ni_{0.2}Mo_{0.8}$ N		1 M KOH	\	218 @ 10	55	[75]
$NiCo_2$N-NF		1 M KOH	\	149 @ 10	65	[76]
Co_3FeNx		1 M KOH	\	222 @ 20	46	[77]
Ni–Fe-MoN		1 M KOH	\	228 @ 100	41	[78]
Cu_3N@CoNiCHs@CF		1 M KOH	\	155 @ 10	96	[79]
MoS_2/NiS_2	Metal sulfides	1 M KOH	\	278 @ 10	91.7	[80]
MoS_2		1 M KOH	\	276 @ 10	81	[67]
$Ni_{1.9}FeS_{1.09}(OH)_{4.6}$		0.1 M KOH	\	162 @ 10	53	[81]
$Co_{1.8}Ni(OH)_{5.6}$@$Co_{1.8}NiS_{0.4}(OH)_{4.8}$		0.1 M KOH	\	274 @ 10	45	[69]
NiTe/NiS		1 M KOH	1.5	209 @ 10	49	[70]
NiFe/NF	Metal hydroxides	0.1 M KOH	0.032	270 @ 20	33	[82]
NiFe LDH@NiCoP/NF		1 M KOH	\	157 @ 10	48.6	[83]

Table 1, great progress has been achieved in the investigation of nonprecious metal catalysts for alkaline conditions and efficient water electrolysis during the previous decade.

Nonprecious metal oxide catalysts

Researchers have extensively investigated non-noble metal oxides as alternatives to noble metal-based electrocatalysts for efficient electrochemical hydrolysis due to their availability, low cost, and excellent electrochemical properties. In the field of catalysis, Co is a typical representative because the electrochemical activity of Co_3O_4 is extremely close to that of the noble metal oxide RuO_2, which Co_3O_4 has very superior electrochemical characteristics, as seen in the volcano diagram in Fig. 2 [84]. As a result, cobalt oxide catalysts are regarded as one of the most promising alternatives to noble metal catalysts, and this research focuses on their OER features as well. The electrocatalytic activity of cobalt oxide is primarily determined by its specific surface area and electronic state. Cobalt oxide lumpy materials have low conductivity and specific surface area, resulting in less-than-satisfactory OER performance. Zhao et al. [85] prepared Ce doped Ni-S@$NiMoO_4$ micropillar composites (CeNiS@$NiMoO_4$/NF) on nickel foam by a two-step hydrothermal-electrodeposition method, and the modified materials have excellent OER properties with ultra-low overpotential. Liang et al. produced Co_3O_4 nanocrystals on graphene oxide and dramatically enhanced their OER performance by varying the grain size [60]. Xu et al. [61] first electrodeposited $Co(OH)_2$ on titanium flakes, then obtained Co_3O_4 nanosheets by calcination, and finally etched Co_3O_4 nanosheets with argon plasma to generate effective Co_3O_4-based OER electrocatalysts with oxygen vacancies and a high surface area. By etching with argon plasma, rough, discontinuous, and loose surfaces were observed, as illustrated in Fig. 4a and b, where linked Co_3O_4 nanoparticles were detected. The specific surface area of the Co_3O_4-based OER electrocatalyst was dramatically enhanced. The XPS results of plasma-etched Co_3O_4 nanosheets in Fig. 4c–f show that the Co^{2+}/Co^{3+} ratio changed, increasing the number of oxygen vacancies while changing the electronic state of Co_3O_4; in Fig. 4g and h, the OER performance was greatly improved in 0.1 M NaOH solution, whereas the original Co_3O_4 nanosheets required a potential of 1.77 V with respect to reversible hydrogen electrode (RHE). The plasma-sculpted Co_3O_4 nanosheets have a Tafel slope of 68 mV dec^{-1} and their overpotential is just 1.53 V.

Plasma treatment of the material's surface can not only produce morphology and oxygen vacancies with high specific surface area, but it can also dope elements into the oxygen vacancies without affecting the material's crystal structure. Xiao et al. [86] employed Ar plasma to treat Co_3O_4 with P precursors, allowing P atoms to enter the oxygen vacancies created in situ by Co_3O_4 to produce effective OER electrocatalysts. The TEM and EXAFS oscillations show that P-Co_3O_4 is mostly spinel type, indicating that the doping of P did not disrupt its spinel structure (Fig. 5a, b). The oscillation intensity in Fig. 5c illustrates the distribution of the material atoms, and the oscillation intensity of porous nanosheets exposed to plasma bombardment is lower than that of bulk nanosheets, suggesting that there are more atoms and disorder on the material surface after plasma bombardment. The XAS results (Fig. 5d) reveal that the Co^{2+} (T d) site dominates the catalytic performance of P-Co_3O_4. In addition, the coordination number of P-Co_3O_4 is nearly identical to that of pristine Co_3O_4 and that Ar plasma-treated cavities may efficiently fill the P. At a current density of 10 mA cm^{-2}, the overpotential of the OER of P-Co_3O_4 is 280 mV, showing that it has strong catalytic activity (Fig. 5e). The hydrothermal reduction process, in addition to the plasma technique, may be used to prepare the development of extremely defective nanosheet Co_3O_4 materials and it has an overpotential of 220 mV for OER at a current density of 10 mA cm^{-2} [62].

Aside from Co_3O_4, numerous other oxides have excellent electrocatalytic properties, including NiO [63], MnO_2 [87], WO_3 [64], and ABO_3 [65]. However, the catalytic capabilities of single-metal oxides are insufficient. Multimetal oxides have been designed to synergistically regulate the electronic structure and address the low conductivity issue to further improve catalytic performance. Due to the desirable electronic structure with plentiful active sites, nickel- and cobalt-based oxides doped with additional transition/alkaline elements such as Fe, Zn, and Cu have shown increased catalytic activity in comparison to monometallic oxides [88–90]. OER catalysts of chalcogenide oxides with ABO_3 structures ($LaFeO_3$, $CaFeO_3$, $SrFeO_3$) have been widely investigated. Because of their adjustable features, including composition and electronic structure, chalcogenide oxides are commonly utilized in OER catalysis. Here, A is an alkali and/or rare earth metal, while B is a transition metal. B is located at the center of the octahedra, each octahedron is interconnected by shared corners to form the skeleton of the structure, and A can fill the open space [6, 91]. However, both chalcogenide and conventional oxide catalysts have low electrical conductivity and specific surface area. To address this issue, Liu et al. [92] prepared graded mesoporous/macroporous chalcogenide $La_{0.5}Sr_{0.5}CoO_{3-x}$ (HPN-LSC) nanotubes by electrostatic spinning and annealing to increase their specific surface area, thereby significantly improving OER performance (Fig. 6a, b). To summarize, porous micro- and nanostructures can improve their specific surface area, allowing their catalytic activity to be fully used and compensating for their low charge transfer rate during electrocatalysis. In addition, Zhu et al. [93] highlight a new halogen-chlorine

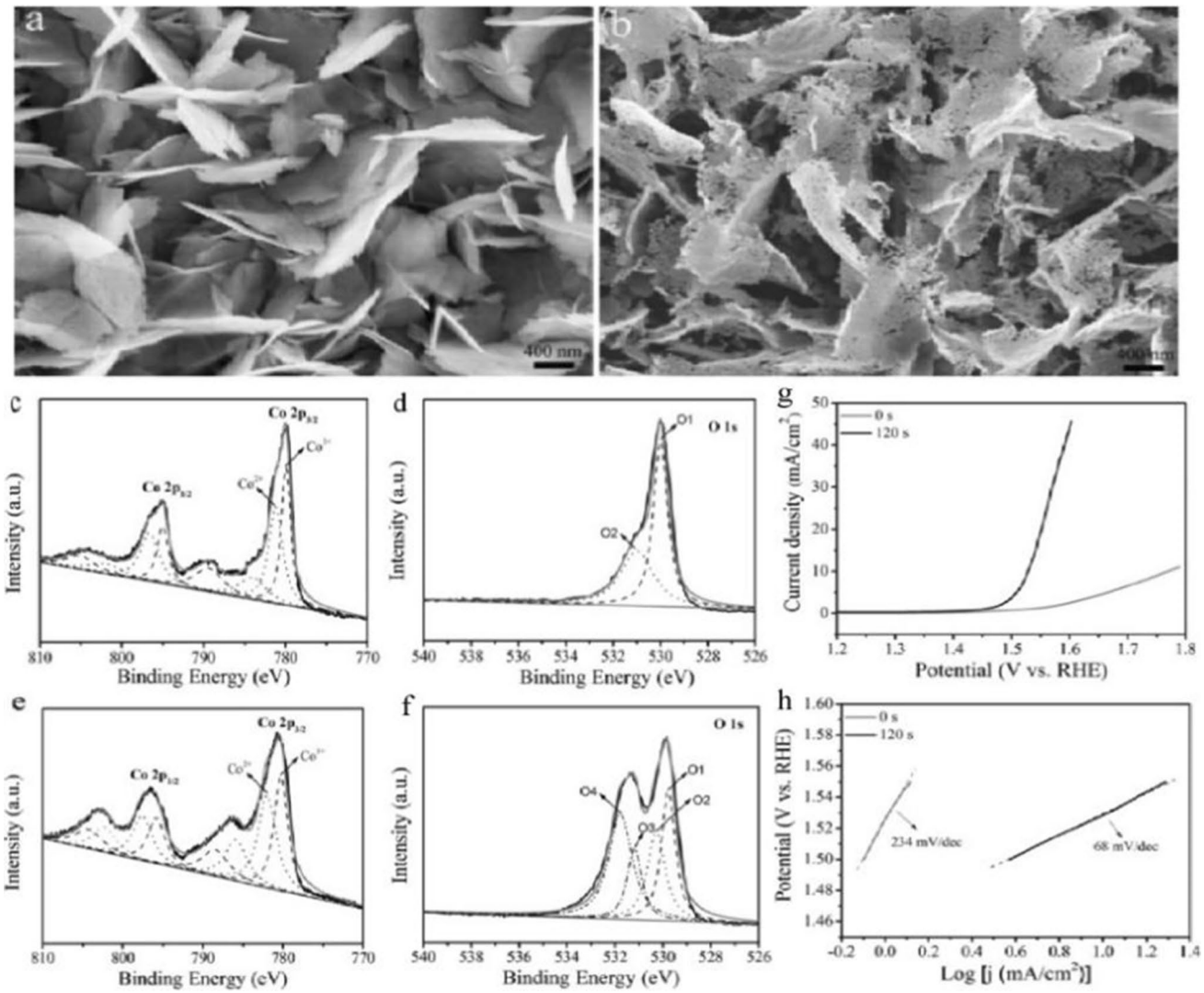

Fig. 4 SEM images of pristine Co_3O_4 (**a**) and Ar-plasma-engraved Co_3O_4 (**b**). XPS images of fitted Co 2p for pristine Co_3O_4 (**c**) and for plasma-engraved Co_3O_4 (**e**). **d**, **f** Fitted O 1 s for pristine Co_3O_4 (**d**) and plasma-engraved Co_3O_4 (**e**). **g** The polarization curves of OER on pristine Co_3O_4 (0 s) and the plasma-engraved Co_3O_4 (120 s). **h** Tafel plots. Reproduced with permission from Ref. [61]

(Cl)-anion doping strategy to boost the OER activity of perovskite oxides.

MOF-derived carbon-based materials for OER

Carbon materials provide excellent OER catalytic characteristics and have been utilized for decades in OER. They are, however, easily oxidized during labor, causing their own structure to disintegrate [94]. MOF-derived carbon compounds are a new kind of crystalline porous materials created by connecting metal ions or clusters with organic linkers [95–97]. They have an open crystal structure, extraordinarily high porosity, structural flexibility, and adjustability. Furthermore, they may supply a large number of active sites while ensuring high-speed electron transport, and it is now recognized as an OER material with high catalytic activity in the field of electrolytic water following considerable study and investigation [98–101]. Zn-based MOFs are one of the most frequently utilized precursors, but their stability performance is poor. Therefore, researchers have employed atomic doping [102] and controlled modular structure creation [103] to increase their catalytic activity and stability. MOFs are becoming increasingly used as catalysts; nevertheless, cobalt-based MOF materials for electrolytic water fields have received the greatest attention [104]. Although Co oxide-based electrocatalysts perform well in the OER, their poor conductivity and proclivity to agglomerate in alkaline environments make them unsatisfactory for commercial applications. Fortunately, it appears that the usage of MOFs as template predecessors can alleviate some of

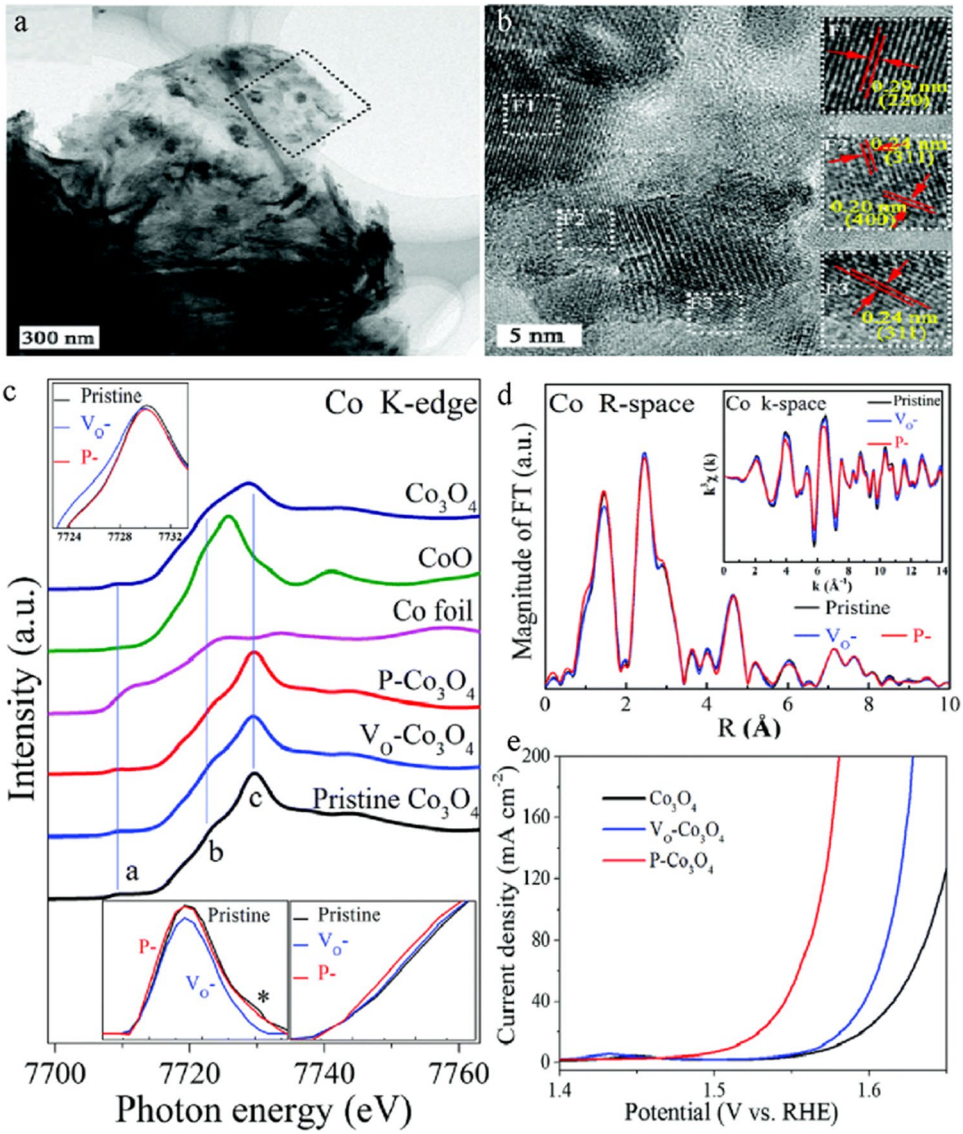

Fig. 5 **a**, **b** TEM images of P-Co_3O_4 at low and high resolution; **c** Co K-edge XANES spectra of pristine Co_3O_4, VO-Co_3O_4, and P-Co_3O_4. The top inset shows the magnification of the main peak region. Bottom insets show the magnification of the prepeak region; **d** Co K-edge EXAFS. The inset shows the Fourier-transform EXAFS oscillations. **e** The polarization curves of OER on pristine Co_3O_4, VO-Co_3O_4, and P-Co_3O_4. Reproduced with permission from Ref. [86]

these issues. To summarize, this approach prepares MOF-derived bimetallic electrocatalysts with tunable microstructures, compatibility with numerous metal ions, and the ability to achieve uniform dispersion of the produced carbon [105–107].

By one-step pyrolysis of polyaniline films with bimetallic organic frameworks, Lu et al. [66] created a hybrid NF@NC-$CoFe_2O_4$/C NRA (Fig. 7a). It saves time and energy over traditional, sophisticated metal oxide/carbon composite production processes. These porous $CoFe_2O_4$/C NRAs show considerable OER catalytic activity and outstanding long-term stability when grown directly on 3D conducting NF substrates. TEM (Fig. 7b) revealed that the nanorods were made up of porous nanoparticles (NPs) due to their enormous surface area, low density, kinetically beneficial open structure, and surface permeability. Furthermore, $CoFe_2O_4$ NPs are clad with an amorphous carbon layer, which boosts electrical conductivity while limiting dissolution and agglomeration. $CoFe_2O_4$ NPs are covered by an amorphous carbon cladding layer, which increases the electrical conductivity while also inhibiting their dissolution and agglomeration. The presence of the $CoFe_2O_4$ crystalline phase can be clearly seen by HRTEM (Fig. 7b), and the presence of $CoFe_2O_4$ crystals is also demonstrated by XRD (Fig. 7c). At 10 mA cm^{-2}, the electrochemical activity test revealed a minimum overpotential of 240 mV and a Tafel slope of 45 mV dec^{-1} (Fig. 7d, e). After 30 h of polarization, the potential increased by 0.42%, and the surface morphology remained nearly constant after 60 h of catalytic activity at 100 mA cm^{-2} (Fig. 7f, g).

The findings of Lu et al. establish the way for the creation of unique porous hybrid MOF nanostructures with controlled shape and function for next-generation electrocatalysts and possible applications in other technological

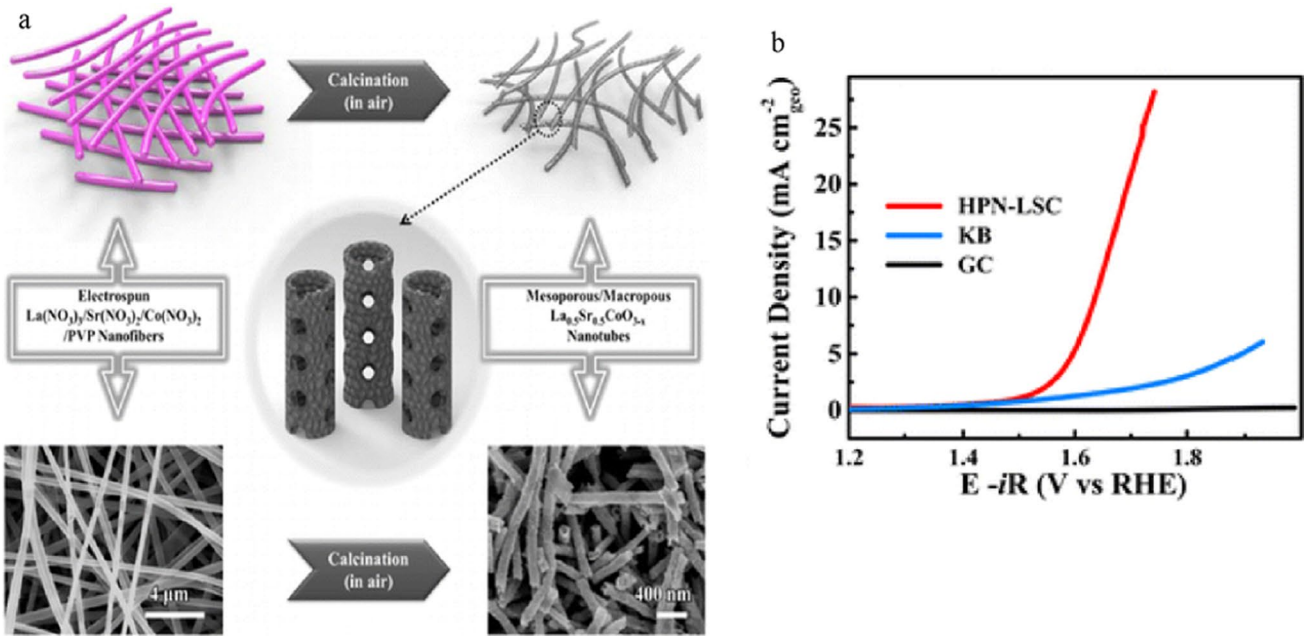

Fig. 6 **a** Schematic illumination of the electrodeposition of $La_{0.5}Sr_{0.5}CoO_{3-x}$; **b** OER polarization curves of glassy carbon (GC), KB, and HPN-LSC catalysts under the same measurement conditions. Reproduced with permission from Ref. [92]

paths. On this basis, Gao et al. [67], by electrochemically polymerizing polyaniline nanowire arrays on carbon paper, growing MOF-74-Co/Fe directly on its surface, and pyrolyzing it to form $CoFe_2O_4$/C loaded on nitrogen-doped carbon nanoarray materials, they created a highly active and stable OER catalyst. Excellent OER activity is ensured by the high specific surface area, high catalyst utilization, increased electron transport capabilities, and conservation of virgin carbon paper qualities (Fig. 8a). Following the electrochemical activity test, it was discovered that it had the lowest overpotential of 152 mV at 10 mA cm^{-2} (Fig. 8b) and a Tafel slope of just 70 mV dec^{-1} (Fig. 8c). Furthermore, NC-$CoFe_2O_4$/C@CP has good mass transport properties, as shown in Fig. 8d. Following an initial current density of 0.25 mA cm^{-2} and working for 21,600 s, the final current density was 0.23 mA cm^{-2}, representing an 8% decrease in current density (Fig. 8e). This shows that the catalyst has excellent stability. The OER process model and the Gibbs free energy change of Co and Fe sites in the $CoFe_2O_4$ structure on the (110) surface were also built (Fig. 8f), and the Gibbs free energy change and DFT calculations revealed that the main surface adsorbent of NC-$CoFe_2O_4$/C@CP is OH*, and the surface Co atom is the main active site. Ling et al. [68] used a hydrothermal process to create Fe_2Ni-MIL-88B MOF (Fe_2Ni MOF/NF) on nickel foam, achieving a current density of 10 mA cm^{-2} at a low overpotential of 222 mV and a very small Tafel slope of 42.39 mV dec^{-1}, with outstanding stability after 50 h of continuous operation. In addition, for OER, MOF hybridization techniques with secondary conducting phases, such as supported substrate graphene [108] and MXenes [69], have also been reported.

In addition to the previously mentioned enhanced specific surface area and electron transport characteristics, ion doping modification is another successful technique for improving MOF catalysts. Li et al. [70] employed a self-templating method to modify the Fe/Ni molar ratio, resulting in Fe/Ni-based MOFs with high activity and stability that can be directly used as efficient OER catalysts (Fig. 9a). The OER activity and stability of the trimetallic Fe/$Ni_{2.4}$/$Mn_{0.4}$-MIL-53 built on the NF substrate were further improved. At a low overpotential of 236 mV and a modest Tafel slope of 52.2 mV dec^{-1}, a current density of 20 mA cm^{-2} was attained (Fig. 9b–d). The exceptional performance can be attributed to the unusual structure and porosity, as well as the synergistic impact of the combined metals. After 100 CV cycles, the electrochemical activity is almost unaltered, indicating high stability (Fig. 9e).

Yuan et al. [71] used an OER catalyst based on the MOF benzotriazole-5-carboxylate (Co_3-btca) to create isomeric bimetallic and trimetallic skeletons by doping with Fe/Ni ions. At 10 mA cm^{-2}, $Co_{2.36}Fe_{0.19}Ni_{0.45}$-btca had a minimal overpotential of 292 mV and a modest Tafel slope of 72.6 mV dec^{-1}. The outstanding catalytic activity is due to the synergistic interaction of the unsaturated coordinated Co, Fe, and Ni sites, which enhances OH adsorption. Converting traditional bulk MOF crystals into two-dimensional nanosheet structures is also incredibly beneficial for improving the performance of OERs [72]. This is because

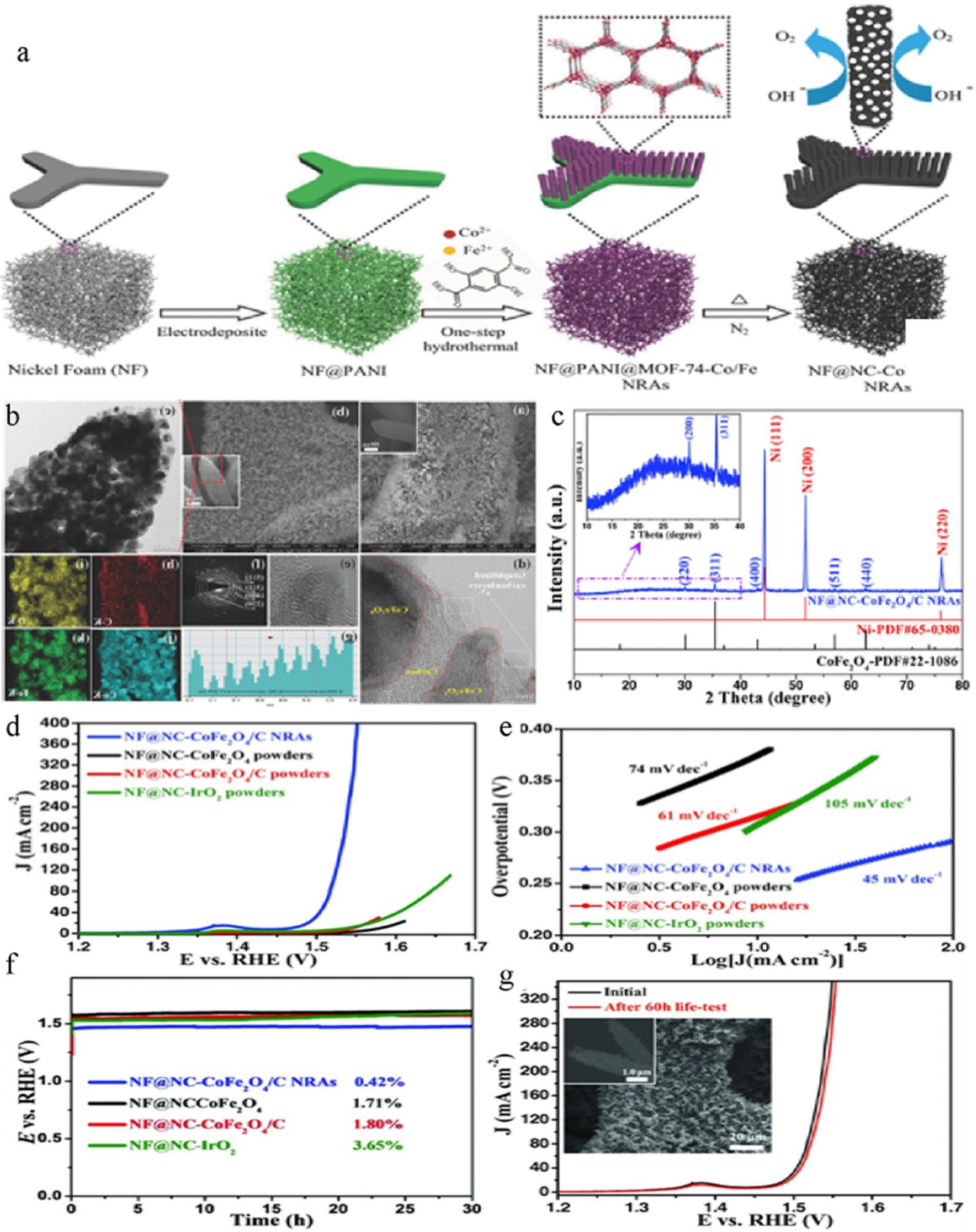
a
Nickel Foam (NF)
Electrodeposite
NF@PANI
One-step hydrothermal
NF@PANI@MOF-74-Co/Fe NRAs
N2
NF@NC-Co NRAs
b
c
Intensity (a.u.)
2 Theta (degree)
Ni(111)
Ni(200)
Ni(220)
NF@NC-CoFe2O4/C NRAs
Ni-PDF#65-0380
CoFe2O4-PDF#22-1086
d
J (mA cm-2)
E vs. RHE (V)
NF@NC-CoFe2O4/C NRAs
NF@NC-CoFe2O4 powders
NF@NC-CoFe2O4/C powders
NF@NC-IrO2 powders
e
Overpotential (V)
Log[J(mA cm-2)]
74 mV dec-1
61 mV dec-1
105 mV dec-1
45 mV dec-1
f
E vs. RHE (V)
Time (h)
NF@NC-CoFe2O4/C NRAs 0.42%
NF@NCCoFe2O4 1.71%
NF@NC-CoFe2O4/C 1.80%
NF@NC-IrO2 3.65%
g
Initial
After 60h life-test
J (mA cm-2)
E vs. RHE (V)

◂**Fig. 7** **a** Schematic illustration showing the one-step PANI-assisted synthesis of bimetal-organic framework NRAs and their derived porous $CoFe_2O_4$/C NRAs; **b** SEM, TEM, HRTEM, and SAED images of MOF-74-Co/Fe NRAs (inset is the magnified MOF-74-Co/Fe nanorod); **c** XRD pattern of NF@NC-$CoFe_2O_4$/C NRAs; **d** LSV curves, **e** Tafel plots, and **f** chronopotentiometry curves of NF@NC-$CoFe_2O_4$/C NRAs, NF@NC-$CoFe_2O_4$ powders, NF@NC-$CoFe_2O_4$/C powders, and NF@NC-IrO_2 powders with the same mass loadings of ≈1.03 mg cm^{-2} in 1.0 M KOH solution at a current density of 10 mA cm^{-2}. **g** LSV curves of NF@NC-$CoFe_2O_4$/C NRAs before and after the 60-h durability test at 100 mA $cm.^{-2}$ (inset: SEM images of the catalyst after the durability test). Reproduced with permission from Ref. [66]

two-dimensional (2D) nanomaterials have a large percentage of active atoms exposed to the working environment, ensuring strong catalytic activity, while their nanoscale size enables quick mass and charge transfer [73, 109]. Notably, the stability of MOFs during OER and the actual catalytic process have received less attention and should be researched further.

Metal nitrides for OER

One of these frontier possibilities might be employed as a catalyst for the electrolysis generation of low-cost hydrogen due to its capacity to execute oxygen evolution reactions at relatively low overpotentials. Due to their noble metal-like characteristics and metallic conductivity, as well as their strong OER activity, metal nitrides have attracted much interest as one of the most efficient frontier electrocatalysts [110]. The density of states (DOS) of Co_4N crosses the Fermi energy level according to DFT calculations, indicating that Co_4N exhibits metallic characteristics and resistive features typical of metals (Fig. 10a) [74]. Typically, nanometallic nitrides are prepared by heating metal oxide or hydroxide precursors in a variety of nitrogen sources (such as NH_3, N_2, NH_2NH_2, urea, and dicyandiamide) [111–113]. However, conventional nitriding takes a long period, and Zhang et al. [111] employed N_2 RF plasma treatment to transform cobalt oxide precursors into cobalt nitride nanowires. When compared to the typical high-temperature NH_3 annealing procedure, this approach takes approximately 1 min at room temperature to obtain the nitride (several hours). The plasma treatment not only significantly decreases the nitriding time while increasing the surface roughness but also achieves a current density of 10 mA cm^{-2} at a low overpotential of 290 mV, a tiny Tafel slope, and a high lifetime in alkaline electrolytes.

Metal nitrides have a lower overpotential than oxides and can be excellent OER catalysts. Elemental doping is a useful method for improving catalyst stability and catalytic performance, and Fe, Ni, Co, and Mo are low-cost metal precursors that are widely utilized with catalysts. The form of nanocatalysts also allows for additional improvement in efficiency. Researchers have demonstrated that multinitrides generated by altering the structure of nitrides, such as Ni-Mo nitride nanorods, Ni-Co nitride nanosheets, Co-Fe nitride nanowires, and Fe–Ni-Mo nitride nanotubes, have good OER catalytic performance and stability [75–78].

In comparison to the other strategies discussed, the heterostructure engineering strategy appears to be the most promising because of the accompanying interfacial effects that contribute to improving electron transfer, optimizing adsorption of key intermediates, and accelerating kinetics caused by the modified electronic structure. Liu [79] used a three-step technique to create 3D layered Cu_3N@CoNiCHs@CF (Fig. 10b), beginning with the oxidation of Cu foam, followed by nitriding treatment, and finally a hydrothermal reaction. The Cu_3N@CoNiCHs@CF produced by the approach has a uniform nanowire structure, and the doping components are dispersed uniformly across the heterostructure (Fig. 10c). The Cu_3N@CoNiCHs@CF electrode has good hydrophilic qualities for more effective electrolyte and ion interactions, and it may minimize bubble adhesion and expedite bubble detachment, which is useful for preserving the electrode's integrity and long-term stability (Fig. 10d). According to the polarization curve in Fig. 10e, Cu_3N@CoNiCHs@CF requires a low overpotential of 155 mV during the OER to obtain a current density of 10 mA cm^{-2}, which is better than IrO_2/CF (330 mV). The Tafel charts of Fig. 10f show similar behavior, with the Tafel slope of Cu_3N@CoNiCHs@CF being 96 mV dec^{-1} with negligible voltage decay after 24 h of polarization at a current density of 10 mA cm^{-2} (Fig. 10g).

Metal sulfides for OER

Among the many potential candidates, transition metal sulfides (TMS), such as MoS_2, CoS_2, and NiS_2, have attracted much interest due to their promising electrocatalytic capabilities, but their restricted active sites and poor stability make them severely limited in their applications [80, 114, 115]. Ion modulation is a powerful technique for improving the characteristics and stability of metal sulfides. Metal hydroxysulfides, for example, are highly active, persistent, and environmentally friendly, and the electrocatalytic performance of *p*-hydroxysulfide catalysts can be improved by introducing sulfur anions into metal hydroxides to modulate the interaction between cations and anions via moderate anions [116]. Wang [81] and colleagues' anion-conditioned NiFe hydroxysulfides were produced in situ on 3D conductive nickel foam by 60-s electrodeposition of NiFe layered double hydroxides. The resulting monoliths (dubbed $Ni_{1.9}FeS_{1.09}(OH)_{4.6}$) were made by immersing the $Ni_{2.3}Fe(OH)_{7.6}$ precursors in a 2.0 m Na_2S solution at 25 °C for 1.0 h, during which the NiFe hydroxides were controllably converted to hydroxysulfides under very mild conditions,

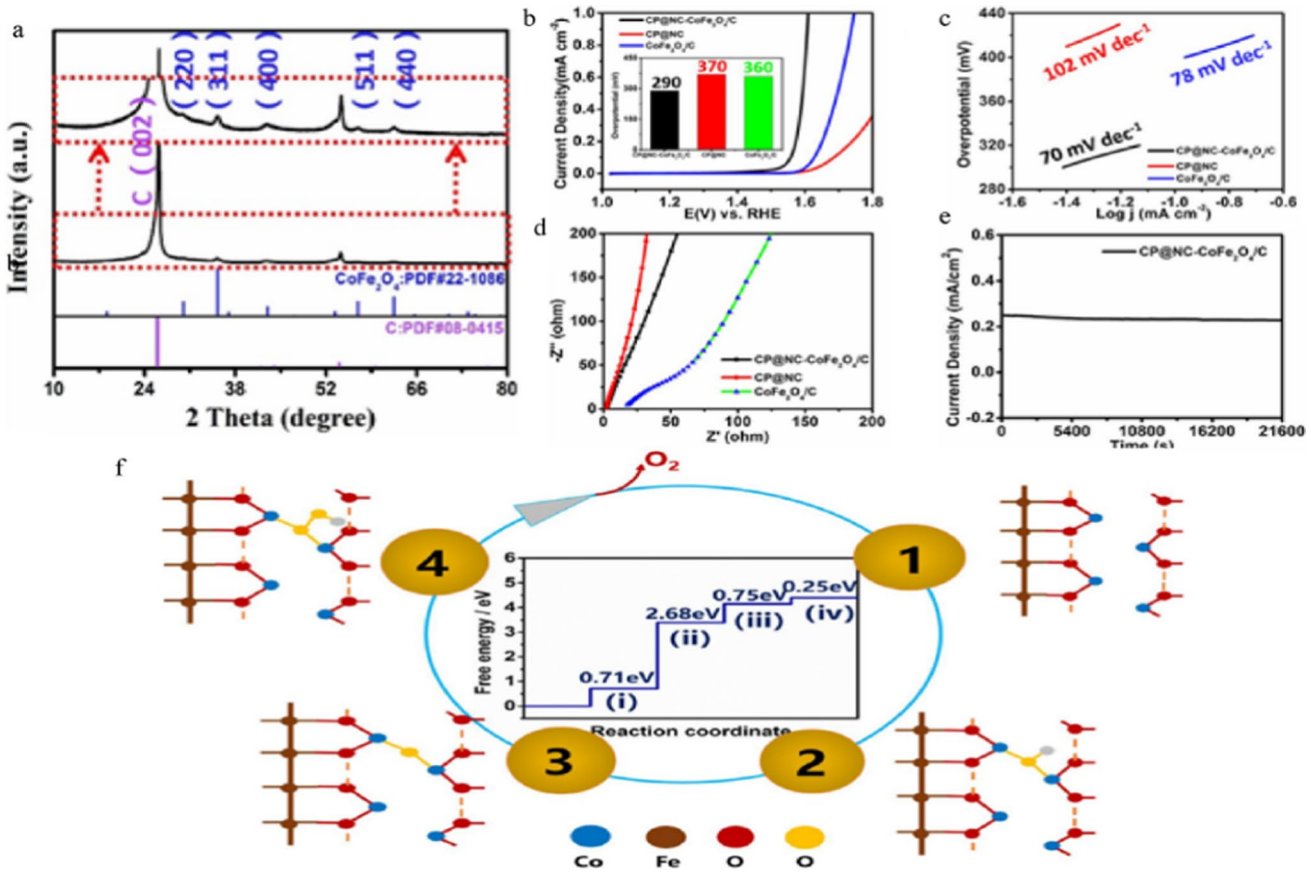

Fig. 8 **a** XRD pattern (partially enlarged) of NC-$CoFe_2O_4$/C@CP; **b** LSV curves of NC-$CoFe_2O_4$/C@CP (black), NC@CP (red), and $CoFe_2O_4$/C (blue) (inset: overpotential histogram); **c** Tafel plots of NC-$CoFe_2O_4$/C@CP (black), NC@CP (red), and $CoFe_2O_4$/C (blue); **d** EIS of NC-$CoFe_2O_4$/C@CP (black), NC@CP (red), and $CoFe_2O_4$/C (blue); **e** chronoamperometric measurement in 1.0 M KOH at 0.54 V (vs. Ag/AgCl). **f** The model of OER process on Co sites in the structure of $CoFe_2O_4$ with [114] orientation. The Gibbs free energy change of each reaction step involved in the OER process. Reproduced with permission from Ref. [67]

as shown schematically in Fig. 11a. These nanosheets were vertically interconnected and self-assembled into 3D nanostructures, facilitating electron transfer and high exposure of active sites to the reactants, and the hexagonal lamellar structure of the hydroxide was well preserved after the controlled sulfidation process. Energy-dispersive spectroscopy (EDS) mapping further illustrated the uniform distribution of sulfur on the hydroxysulfide nanosheets (Fig. 11b). Furthermore, XPS spectroscopy shows that S synergizes with Fe, Ni, and O and that the shape and crystalline phase of NiFe hydroxides are effectively retained following the room temperature sulfidation process. The OER activity of $Ni_{1.9}FeS_{1.09}(OH)_{4.6}$ is even better than that of the Ir/C catalyst, with a negative shift of more than 80 mV (Fig. 11c). The overpotential required for 10 mA cm^{-2} was lowered by 162 mV for OER. Furthermore, $Ni_{1.9}FeS_{1.09}(OH)_{4.6}$ had a low Tafel slope of 53 mV dec^{-1} (Fig. 11d), which was slightly lower than that of Ir/C (56 mV dec^{-1}) and demonstrates $Ni_{1.9}FeS_{1.09}(OH)_{4.6}$ as an efficient OER catalyst.

In subsequent research, the team exploited core–shell heterostructures to improve the catalytic performance of nonprecious metals. For maximum performance, core–shell heterostructures can provide robust mechanical features that restrict the entire exposure of active areas with high inherent reactivity and extrinsic physicochemical attributes. An ethanol-modified surface vulcanization approach was used to create nanosized CoNi hydroxide@hydroxysulfide core–shell heterostructures. The developed hydroxide@hydroxysulfide core-shells were shown to be a good OER catalyst, with a minimal overpotential of 274.0 mV needed for 10.0 mA cm^{-2}, a low Tafel slope of 45.0 mV dec^{-1}, and long-term stability in 0.10 M KOH [117]. Defects in bimetallic sulfide hybrids influence the electrical behavior and, hence, the electrocatalytic characteristics. Lin and colleagues [80] developed and produced faulty heterogeneous nanosheets with numerous electroactive sites directly on conducting substrates for monolithic hydrolysis. Xue and colleagues [118] initially developed NiTe nanoarrays on NF using a hydrothermal approach and then used an ion-exchange procedure to create NiTe/NiS heterojunctions. For nonhomogeneous electrocatalytic processes, the catalytic performance of the electrocatalyst is mostly determined by

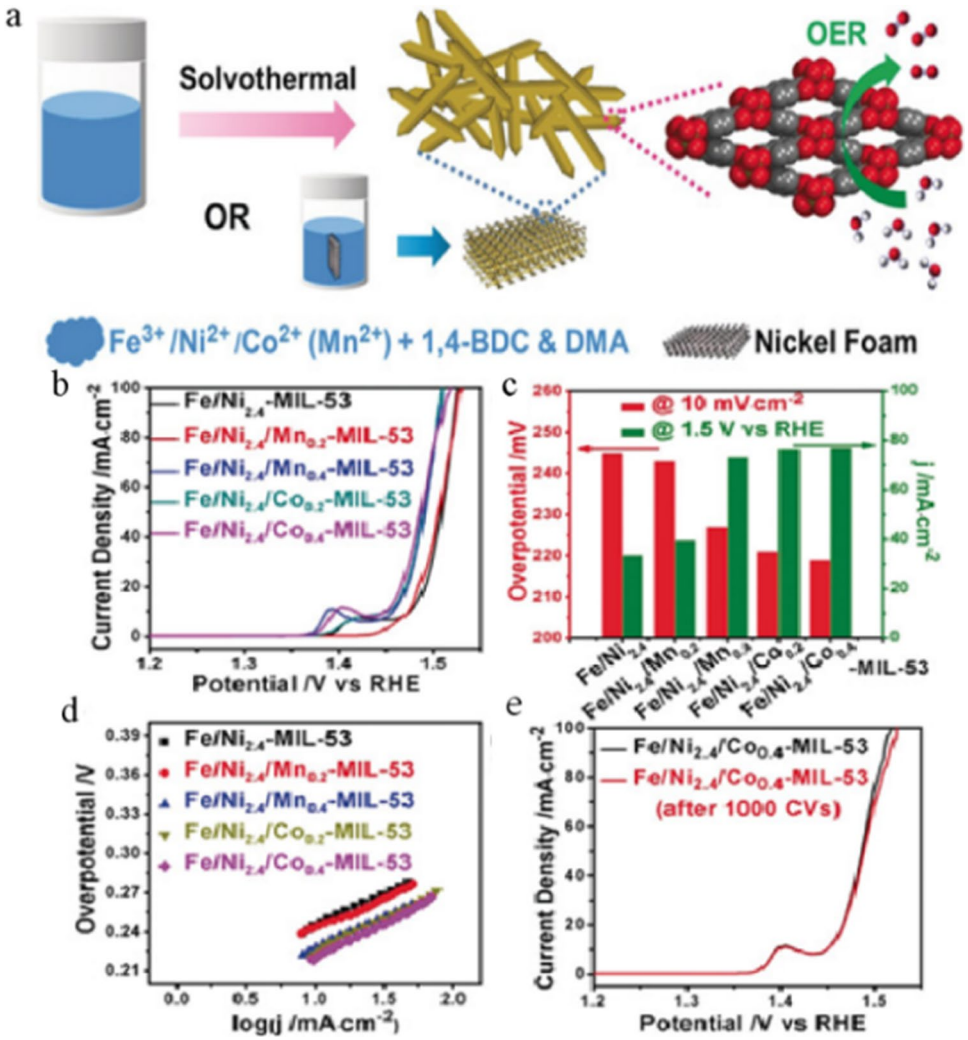

Fig. 9 **a** Schematic illustration of the preparation of Fe/Ni/Co(Mn)-MIL-53 and Fe/Ni/Co(Mn)-MIL-53/NF; **b** OER polarization curves of Fe/$Ni_{2.4}$-MIL-53 and Fe/$Ni_{2.4}$/Mx-MIL-53 (M = Co, Mn; x = 0.2, 0.4); **c** the corresponding overpotential and current density of different catalysts at 10 mA $cm.^{-2}$ and 1.5 V versus the reversible hydrogen electrode (RHE), respectively. **d** Tafel plots of different catalysts. **e** Polarization curves of Fe/$Ni_{2.4}$/$Co_{0.4}$-MIL-53 before and after 1000 cycles. Reproduced with permission from Ref. [70]

the interfacial characteristics of the material. A great catalyst should have a reaction intermediate adsorption energy on the material surface that is neither too strong nor too weak [119]. As a result, optimizing intermediates in the interface engineering strategy to increase adsorption behavior on the material surface is critical to improving catalytic performance.

Metal hydroxides/oxyhydroxides for OER

Metal hydroxides are considered a member of the large family of two-dimensional (2D) materials, and nanostructured layered double hydroxides (nLDHs) have made significant processes and continuous breakthroughs for OER electrocatalysis in recent years due to their high catalytic activity, high active specific surface area, and high stability [120–123]. However, like with metal oxides, there is the issue of relatively low electrical conductivity. To address this issue, researchers typically place it on a conductive substrate, which not only enhances conductivity but also gives more catalytic sites [124–126]. NiFe LDH is considered a benchmark for OER in alkaline media. As a result, researchers considered loading it with other highly conductive substrates. Yuan et al. [127] successfully constructed graded core–shell NiCo2S4@CoNi-LDH nanoarrays with excellent oxygen precipitation reaction (OER) electrocatalytic activity grown on carbon cloth (CC) by a three-step hydrothermal strategy. Wang and colleagues [128] employed electrodeposition to deposit Ni–Fe hydroxyl oxide catalysts on carbon paper. Daniel and colleagues [129] employed an electron beam evaporator to create (Ni,Fe)OOH catalysts by metal deposition of Ti and Au on a substrate. Lu and colleagues [82] electrodeposited layered structured three-dimensional (3D) oxygen electrodes with exceptionally high specific surface area, conductivity, and integrity on nickel foam amorphous mesoporous nickel hydroxide (NiFe) nanosheets. Tang et al. [83] spatially confined growth of nano-sized NiFe LDHs into a 3D graphene framework via defect-anchored nucleation, which was shown to outperform commercial Ir/C catalysts. Zhang and colleagues [130]

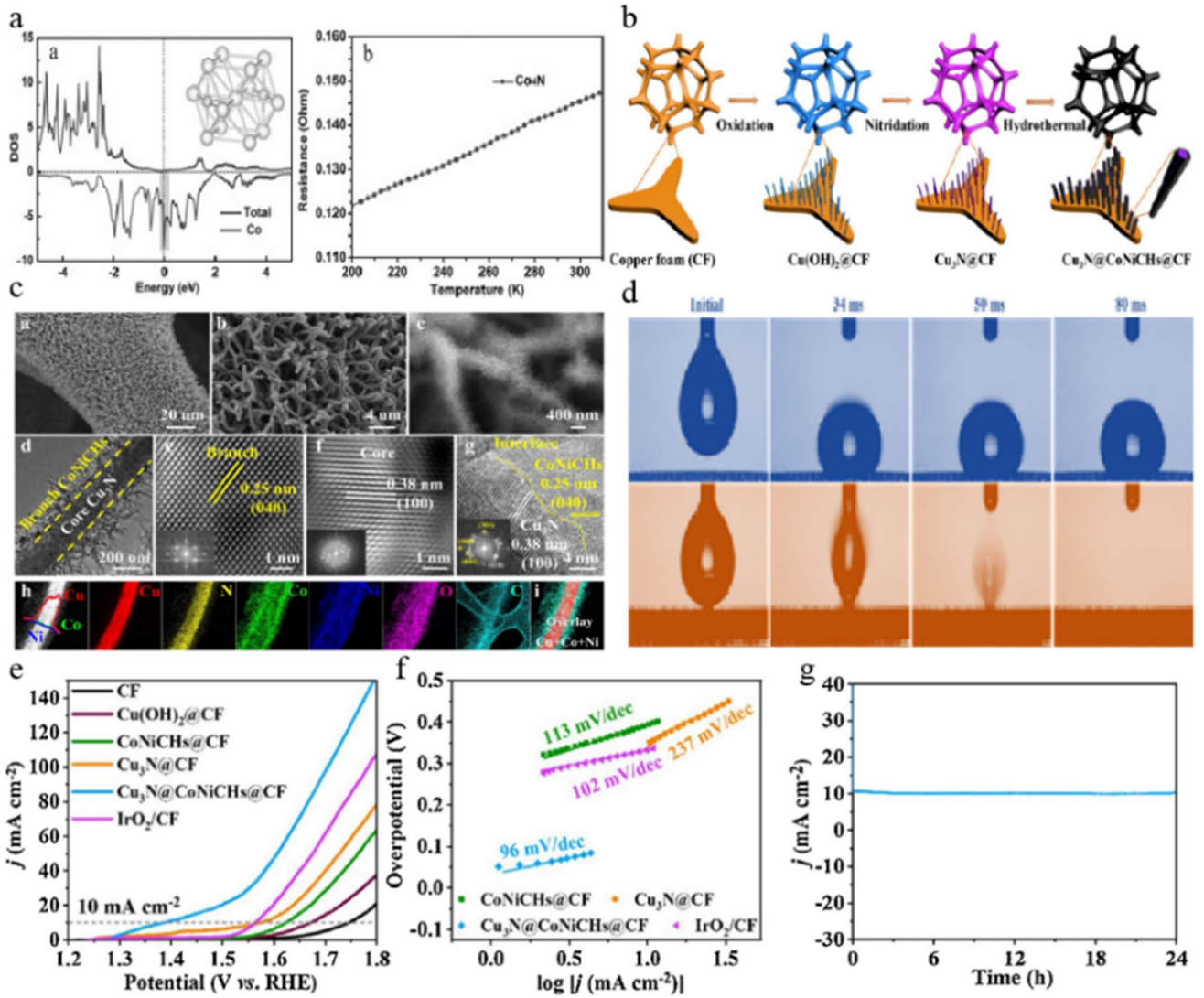

Fig. 10 **a** Calculated density of states (DOS) for Co_4N product. Inset: corresponding crystal structure of Co_4N product with dominant Co–Co metallic bonds and temperature-dependent electrical resistance of Co_4N product; **b** schematic illustration for the synthesis of Cu_3N@CoNiCHs@CF; **c** SEM, TEM, HRTEM, SAED, and STEM images of Cu_3N@CoNiCHs and its elemental mapping images, overlay mapping of Cu, Co, and Ni elements; **d** wettability test of CF and Cu_3N@CoNiCHs@CF electrode; **e** polarization curves; **f** corresponding Tafel plots; **g** chronoamperometry curve of Cu_3N@CoNiCHs@CF for OER. Reproduced with permission from Ref. [74, 79]

initially hydrothermally produced NiCo hydroxide nanowires on NF with a porous 3D structure to be employed as current collectors in a three-step hydrothermal technique to increase the OER performance of NiFe LDH materials. These NiCo hydroxide nanowires were then phosphorylated to produce NiCoP nanowires. Finally, an additional hydrothermal reaction was used to generate NiFe LDH nanosheets on top of these NiCoP nanowires, as illustrated schematically in Fig. 12a, c, and d. The crystal changes of the electrode-posited Co species were confirmed after calcination treatment (Fig. 12b). At a current density of 10 mA cm^{-2}, the electrode had a low overpotential of 220 mV compared to 240, 250, and 330 mV for NiFe LDH/NF, NiCoP/NF, and bare NF, respectively. In addition, the electrode has a minimum Tafel slope of 48.6 mV dec^{-1} (Fig. 12f), showing that NiFe LDH@NiCoP/NF has quicker OER kinetics. A long-term chronopotentiometry experiment at a current density of 10 mA cm^{-2} for 100 h was performed to examine the stability of the NiFe LDH@NiCoP/NF electrode for the OER (Fig. 12g). It is worth researching why in situ hydroxides have higher OER activity than directly manufactured catalysts, and the cause of the discrepancy should be researched further. In addition, it is important to understand how the exposed surface of LDH affects its electrocatalytic activity. Zhang et al. [131] elucidate the active edge surfaces of LDHs for OER by combining molecular probe methods and

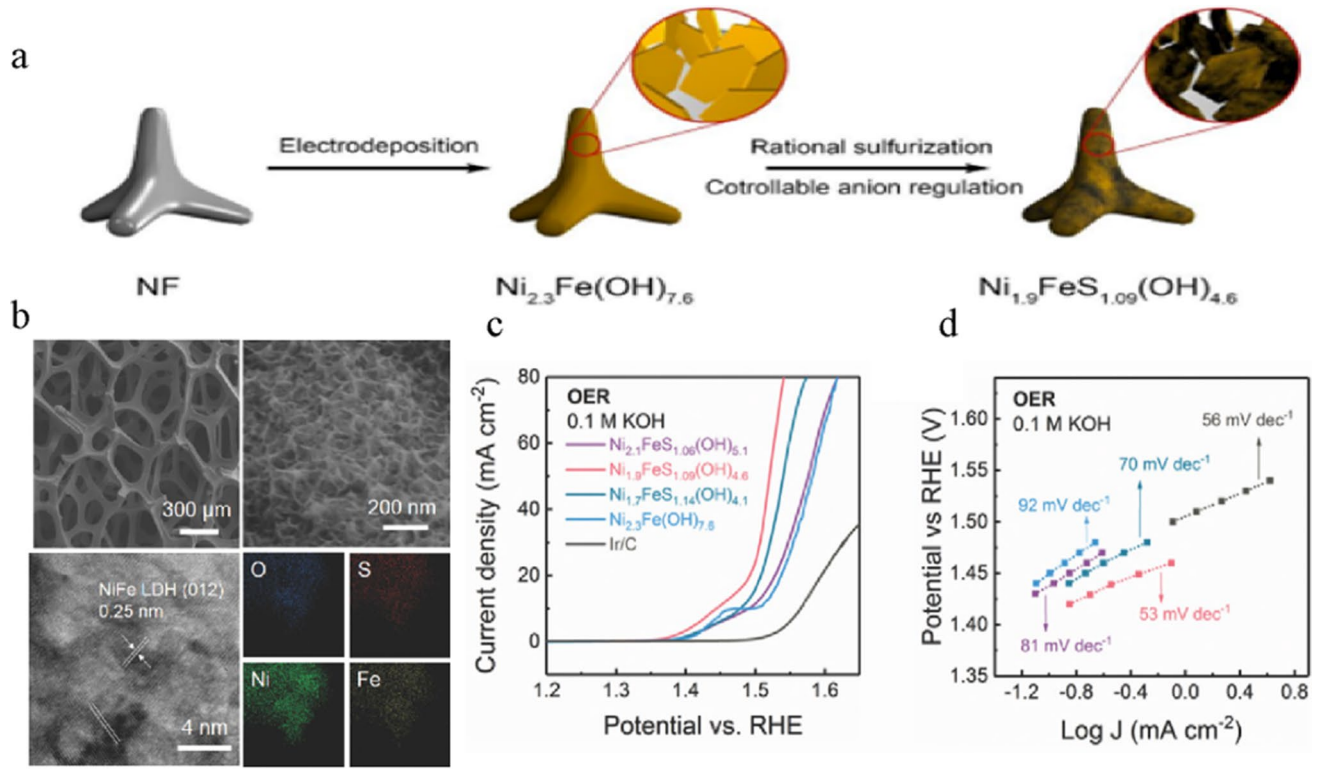

Fig. 11 **a** Illustration of the fabrication of the $Ni_{1.9}FeS_{1.09}(OH)_{4.6}$ hydroxysulfide monolith; **b** morphology and structural characterization of $Ni_{1.9}FeS_{1.09}(OH)_{4.6}$ SEM images, TEM images, and EDS mapping; **c** OER LSV plots; **d** OER Tafel plots. Reproduced with permission from Ref. [81]

fine control of computationally computed edge-to-surface ratios. It provides guidance for us to understand the impact of LDH exposure on OER.

High-entropy materials for OER

Cantor et al. and Yeh et al. developed the notion of high-entropy alloys (HEAs) in 2004. HEAs are multi-principal alloys having at least five elements with atomic concentrations ranging from 5 to 35% of each element [132–134] or characterized in terms of mixed entropy. HEAs offer outstanding mechanical qualities (high hardness, high thermal stability, wear resistance, fracture resistance, and exceptional high elongation) [135, 136]. Because of HEAs' high compositional tunability, the composition may be altered to some extent on the electrical and geometrical structure, allowing HEAs to demonstrate outstanding catalytic characteristics in the field of electrocatalysis as well. Furthermore, the high number of atomic arrangements on the catalytic surface of HEAs can provide a diversity of surface locations relevant to the adsorption, activation, and conversion of reactants and associated intermediates, enhancing electrocatalytic activity. HEA has strong structural stability due to its high entropic stability, which helps increase electrocatalytic stability [137].

To the best of our knowledge, a large number of studies have indicated that NiFe, CoFe, and NiCoFe-based materials are the best non-noble metal OER electrocatalysts reported in the past few years[138]. Cui et al. [139] discovered experimentally that FeNiMnCrCu HEA has greater OER performance than FeCoNiCrAl HEA in order to demonstrate that elemental manipulation may increase the OER ability of HEAs. When the crystal structures of the two were compared, it was discovered that higher radii of Cu and Mn rather than Al and Co permitted the mixing of FCC and BCC phases, resulting in more residual strain. Cu had the ability to eliminate d vacancies, but Mn had a strong attraction for O atoms. Furthermore, a sufficient number of d vacancies can efficiently speed electron transport, matching lattice spacing aids reactant absorption and product desorption, and significant residual strain aids in activating OER at low overpotential. This implies that modifying the composition of HEAs can be employed for electrocatalytic applications. In recent years, Qiu et al. [140] produced a variety of nanoporous HEAs materials using FeCoNi as the starting material and investigated the effect of elemental composition modification on electrochemical characteristics by varying

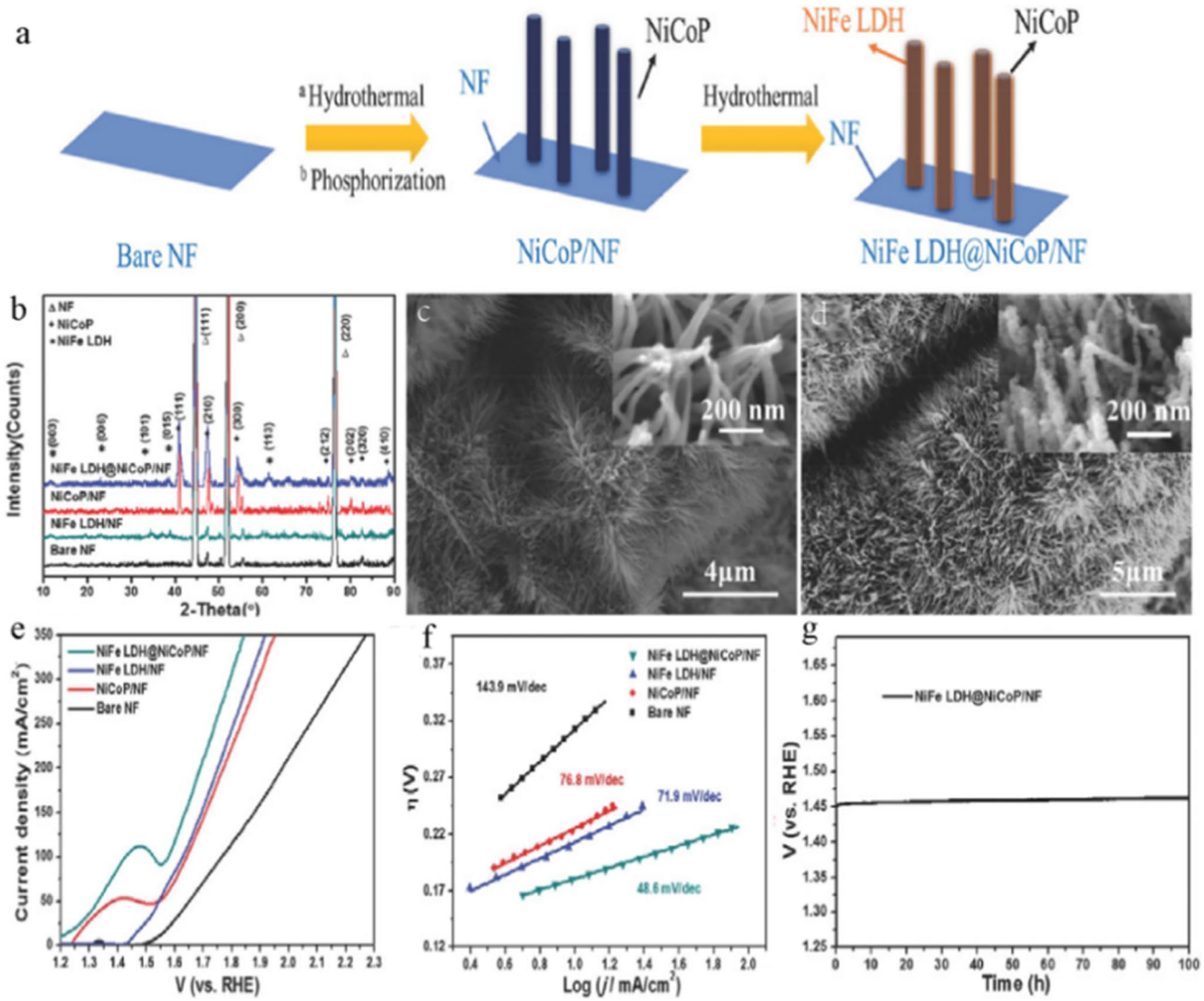

Fig. 12 **a** Schematic representation of the synthesis of 3D hierarchical NiFe LDH@NiCoP/NF electrodes; **b** XRD spectra of the bare NF, NiCoP/NF, NiFe LDH@NiCoP/NF, and NiFe LDH/NF; **c** SEM image of the as-synthesized NiCoP/NF nanowires, where the inset shows a high-resolution image of the NiCoP nanowires; **d** SEM image of the as-synthesized NiFe LDH@NiCoP/NF nanowires, where the inset shows a high-resolution image of the NiFe LDH@NiCoP nanowires; **e** OER LSV plots; **f** OER Tafel plots; **g** long-term stability test of the NiFe LDH@NiCoP/NF for the OER carried out at a constant current density of 10 mA cm.$^{-2}$. Reproduced with permission from Ref. [130]

the fourth and fifth elements compositions. Electrochemical experiments revealed that FeCoNiFeMo HEAs had the highest OER activity. At a current density of 10 mA cm^{-2} and a Tafel slope of 46 mV dec^{-1}, the oxygen precipitation overpotential was only 240 mV. (Fig. 13a, b). After 50 h of polarization testing, the surface morphology of the HEAs remained unchanged (Fig. 13c). HRTEM and STEM-EDS analyses indicated that the elemental distribution of the HEAs remained constant after 50 h of polarization, and a thin coating developed on the HEAs surface due to natural oxidation (Fig. 13d). This occurrence suggests that the OER active site is an in situ rebuilt oxide layer on the surface of the HEAs (under electrochemical circumstances), rather than the HEAs' original surface. During the same time period, Dai et al. [141] produced MnFeCoNi HEA through mechanical alloying and activated MnFeCoNi HEA using electrochemical cyclic voltammetry scanning (CV). Composite MOx (M = Mn, Fe, Co, and Ni) nanosheets were formed on the surface of MnFeCoNi HEA particles to form a core–shell structure, which dramatically increased surface area and active sites, resulting in significantly improved OER activity. The MnFeCoNi HEA working electrode obtained an overpotential of 302 mV with CV activation at a current density of 10 mA cm^{-2} and a Tafel slope of just 83.7 mV dec^{-1}. The findings of their study are consistent with those of Qiu et al. This also presents research ideas for

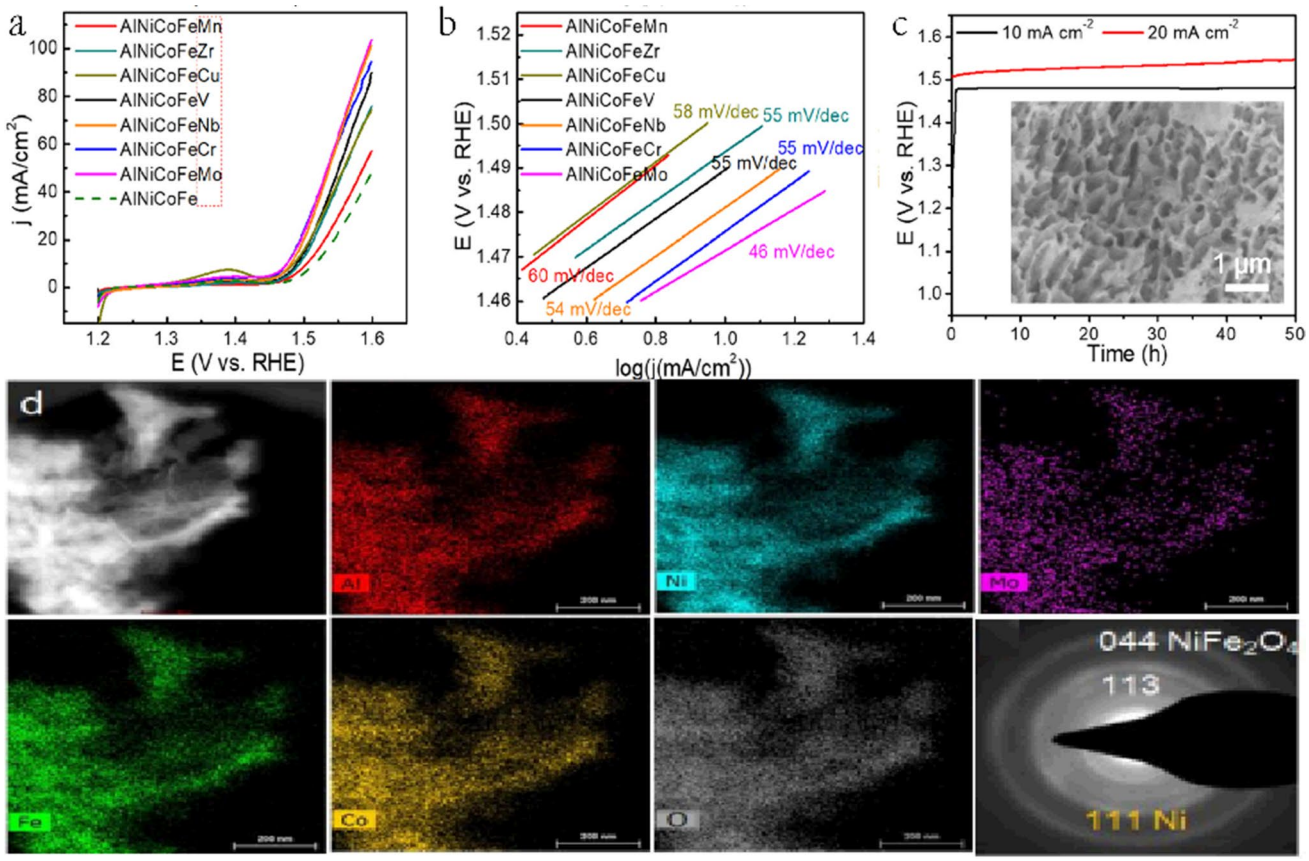

Fig. 13 **a** LSV curves showing the oxygen evolutions on the np-HEAs, np-AlNiCoFe. **b** The corresponding Tafel curves. **c** The inset is the SEM image after 50 h of testing. 1.0 M KOH solution was used for all these tests. **d** STEM-EDS mapping and the np-AlNiCoFeMo sample after 50 h of testing. The results show no obvious morphology or crystal structure changes after the testing. The five metal elements distribute uniformly in the np-HEA/HEO. Reproduced with permission from Ref. [140]

future investigations, which are no longer confined to HEAs for catalysis but may also use high entropy oxides (HEOs) for OER catalysis [142]. Ding et al. created a core–shell nanostructure comprising amorphous HEO ultrathin films for highly reactive OER in a subsequent work [143].

Although high-entropy alloys offer significant benefits in the field of OER, most experimental research are still in the trial-and-error stage, making it difficult to investigate the controlled synthesis of multiple elements. With the emergence of analog computing, it gives assistance in the field of OER for the controlled synthesis of high-entropy alloys [137]. Yao et al. [144] report the computationally aided, entropy-driven design and synthesis of highly efficient and durable catalyst MEA-NPs. The computational strategy includes prescreening of millions of compositions, prediction of alloy formation by density functional theory calculations, and examination of structural stability by a hybrid Monte Carlo and molecular dynamics method. Zhang et al. [145] used density functional theory (DFT) to estimate catalytic performance by developing reaction models, and their results broadened the notion of high entropy alloys. The schematic depiction of the adsorption geometries associated to the intermediates with the elemental components is shown in Fig. 14a. The theoretical calculation (Fig. 14b) indicated the rate determining step to be the transition from adsorbed OH (OH*) to adsorbed O (O*) based on the reaction free energies. As a result, a unique low-temperature electrochemical reconstruction approach is used to create innovative high-entropy Co–Cu–Fe–Mo (oxy)hydroxide electrocatalysts (Fig. 14c). These as-prepared quaternary metallic (oxy)hydroxides exhibit significantly better OER performance than ternary Co–Cu–Mo (oxy)hydroxide, Co–Fe–Mo (oxy)hydroxide, and other counterparts, with a low overpotential of 199 mV at a current density of 10 mA cm^{-2} and a 48.8 mV dec^{-1} Tafel slope in 1 M KOH and excellent stability without decay over 72 h.

However, the research of HEM-based electrocatalysts is in the early stage, and there still exist many limitations that require breakthroughs. The controlled synthesis of high-entropy materials, as well as the link between structure and catalytic performance, is a pressing issue that must be addressed.

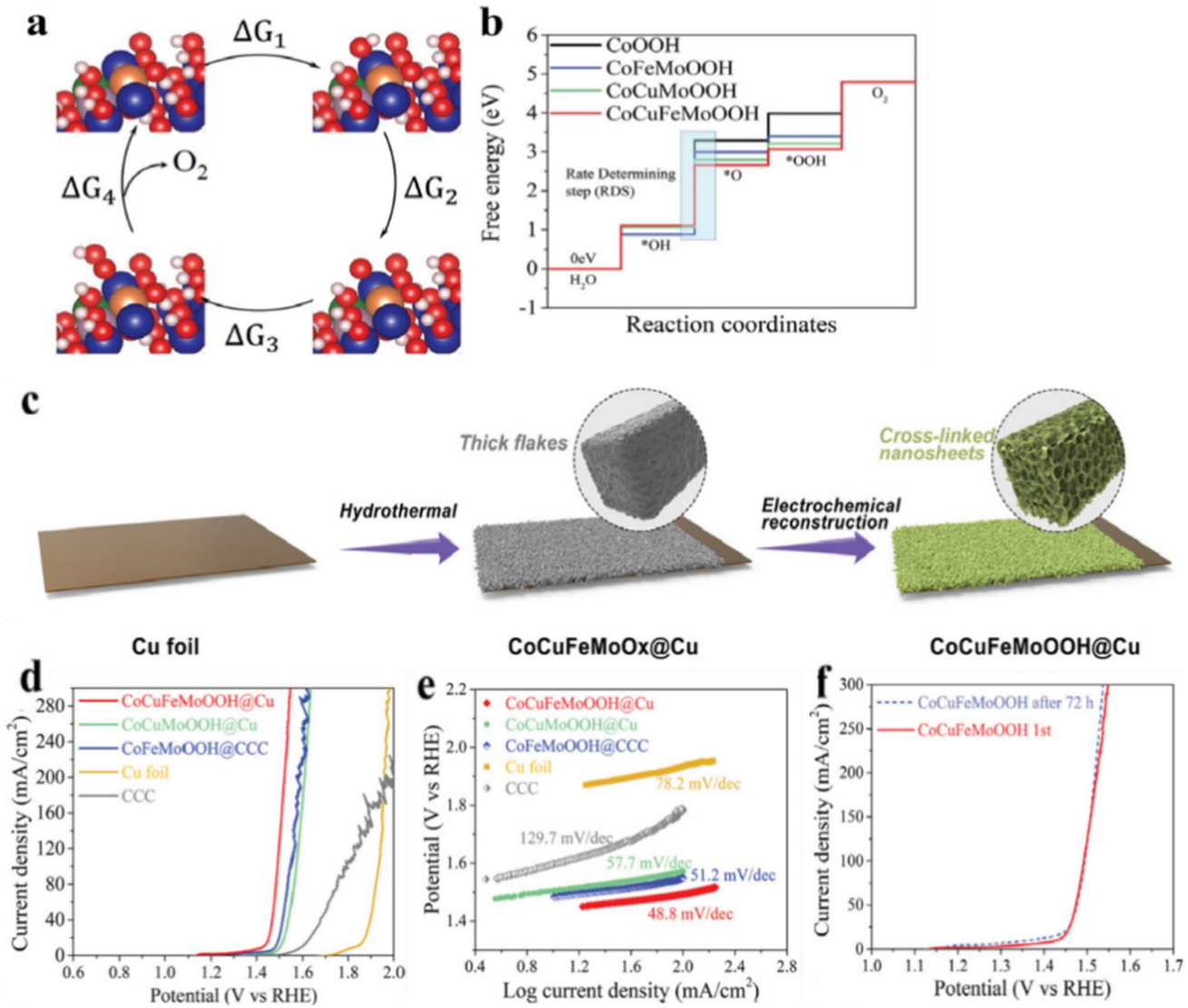

Fig. 14 **a** Adsorption geometries of the intermediates with constitute elements of H (white), O (red), Co (blue), Cu (orange), Fe (green), and Mo (gray). **b** The free energy landscape at 0 V. **c** Schematic illustration of the synthesis of CoCuFeMoOOH@Cu. **d** LSV curves. **e** Tafel plots. **f** LSV curves of CoCuFeMoOOH@Cu before and after 72 h of testing. Reproduced with permission from Ref. [145]

Conclusions and outlook

This paper summarizes the possible uses of several kinds of noble metal-free active materials for electrochemical water oxidation in alkaline environments, including nonprecious metal oxidizing materials, MOF-derived carbon-based materials, material nitrides, material sulfides, and metal hydroxides. The rational design and synthesis (chemical doping; defects (vacancies); phase, facet, and structure) of these electrocatalytic materials can profoundly enhance their OER efficiency. In particular, the construction of heterojunction nanostructures and the connection of active materials with carbon nanocarriers can considerably improve catalytic performance. This is because most electrocatalysts undergo surface phase transitions during in situ electrochemical oxidation during the electrolytic OER of water, providing them with new active sites and labelable catalytic activity. Furthermore, the present research development of new nonprecious metal high-entropy materials in the field of OER is discussed.

Although remarkable milestones have been achieved in the development of electrocatalysts for alkaline environments, some issues still require further investigation. (1) Catalytic activity of catalysts is primarily determined by their own electronic structure or by increasing active sites by designing and preparing nanostructures to increase the specific surface area. However, the structure and phases of catalysts vary dynamically during the reaction process,

and the mechanism of their OER is unclear. It appears that investigating efficient and low-cost synthetic approaches and verifying the real number of active sites in the water electrolysis OER process is critical. The structure–activity–stability relationship on the surface of the catalyst is revealed by theoretical calculations combined with advanced in situ analysis techniques, and the dynamic evolution law of electrocatalytic active species on the surface of the catalyst is revealed, which is useful for the prediction and synthesis of catalysts with excellent catalytic performance. (2) Our capacity to understand the reaction mechanism is currently constrained by the operational/in situ characterization that dominates current research findings. It is highly desirable to combine several effective operational/in situ approaches to enable future advancement of the existing catalysts into advanced catalysts. (3) Many catalysts have been explored, but only a handful have been employed on a wide basis commercially. In the case of large-scale commercial applications, not only material attributes (activity, lifespan, mechanical strength, etc.) but also other factors of the production process must be taken into account, the most significant of which is the material synthesis. Although excellent binders can be found to overcome the durability for industrial applications, the majority of catalysts now available are powder based. Therefore, the development of sophisticated self-supporting electrocatalysts with adequate performance requires the use of novel, straightforward synthetic techniques. Water/solvothermal reactions, galvanic displacement reactions, electrochemical deposition, and fast pyrolysis methods (particularly for high-entropy materials) have all been demonstrated to be effective strategies for controlling the synthesis of catalytic materials with well-structured and reactive interfaces. These techniques allow for in situ growth of the active phase on the carrier, resulting in strong interactions and superior electrical conductivity, and they merit further research for the production of target catalytic materials based on carefully planned and managed synthesis. Furthermore, standard assessment criteria for OER catalysts in alkaline settings are required.

Inspiring and opportunities come with challenges. The development of low-cost nonprecious metal electrocatalysts for large-scale electrolytic water applications under alkaline conditions is expected to be facilitated by a better understanding of the reaction mechanism and the research of the structures and compositions required for material synthesis.

Funding This work was supported by the National Key Research and Development Program of China (Grant 2018YFA0702100) and the National Natural Science Foundation of China (Grant No. 11605116).

Declarations

Conflict of interest The authors declare that they have no known competing financial interests or personal relationships that could have appeared to influence the work reported in this paper.

References

1. Chu S, Majumdar A (2012) Opportunities and challenges for a sustainable energy future. Nature 488(7411):294–303. https://doi.org/10.1038/nature11475
2. Cabán-Acevedo M, Stone ML, Schmidt JR, Thomas JG, Ding Q, Chang HC, Tsai M-L, He J-H, Jin S (2015) Efficient hydrogen evolution catalysis using ternary pyrite-type cobalt phosphosulphide. Nat Mater 14(12):1245–1251. https://doi.org/10.1038/nmat4410
3. Dau H, Limberg C, Reier T, Risch M, Roggan S, Strasser P (2010) The mechanism of water oxidation: from electrolysis via homogeneous to biological catalysis. ChemCatChem 2(7):724–761. https://doi.org/10.1002/cctc.201000126
4. You B, Sun Y (2018) Innovative strategies for electrocatalytic water splitting. Acc Chem Res 51(7):1571–1580. https://doi.org/10.1021/acs.accounts.8b00002
5. Zeng K, Zhang D (2010) Recent progress in alkaline water electrolysis for hydrogen production and applications. Prog Energy Combust Sci 36(3):307–326. https://doi.org/10.1016/j.pecs.2009.11.002
6. Suen NT, Hung SF, Quan Q, Zhang N, Xu YJ, Chen HM (2017) Electrocatalysis for the oxygen evolution reaction: recent development and future perspectives. Chem Soc Rev 46(2):337–365. https://doi.org/10.1039/C6CS00328A
7. Gao R, Zhang Q, Chen H, Chu X, Li GD, Zou X (2020) Efficient acidic oxygen evolution reaction electrocatalyzed by iridium-based 12L-perovskites comprising trinuclear face-shared IrO_6 octahedral strings. J Energy Chem 47:291–298. https://doi.org/10.1016/j.jechem.2020.02.002
8. Over H (2021) Fundamental studies of planar single-crystalline oxide model electrodes (RuO_2, IrO_2) for acidic water splitting. ACS Catal 11(14):8848–8871. https://doi.org/10.1021/acscatal.1c01973
9. Wang C, Zhao J, Du X, Sun S, Yu X, Zhang X, Lu Z, Yang X (2021) Hydrogen production from ammonia borane hydrolysis catalyzed by non-noble metal-based materials: a review. J Mater Sci 56(4):2856–2878. https://doi.org/10.1007/s10853-020-05493-7
10. Wang Y, Yang Y, Wang X, Li P, Shao H, Li T, Liu H, Zheng Q, Hu J, Duan L, Hu L, Liu J (2020) Electro-synthesized $Co(OH)_2$@CoSe with Co-OH active sites for overall water splitting electrocatalysis. Nanoscale Advances 2(2):792–797. https://doi.org/10.1002/aenm.201801926
11. Zhang J, Liu C, Zhang B (2019) Insights into single-atom metal–support interactions in electrocatalytic water splitting. Small Methods 3(9):1800481-1800495. https://doi.org/10.1002/smtd.201800481
12. Qi K, Chhowalla M, Voiry D (2020) Single atom is not alone: metal–support interactions in single-atom catalysis. Mater Today 40:173–192. https://doi.org/10.1016/j.mattod.2020.07.002
13. Siwal SS, Yang W, Zhang Q (2020) Recent progress of precious-metal-free electrocatalysts for efficient water oxidation in acidic media. J Energy Chem 51:113–133. https://doi.org/10.1016/j.jechem.2020.03.079

14. Lei Y, Xu T, Ye S et al (2021) Engineering defect-rich Fe-doped NiO coupled Ni cluster nanotube arrays with excellent oxygen evolution activity. Appl Catal B 285:119809. https://doi.org/10.1016/j.apcatb.2020.119809
15. Ye S, Lei Y, Xu T, Zheng L, Chen Z, Yang X et al (2022) Deeply self-reconstructing CoFe $(H_3O)(PO_4)_2$ to low-crystalline $Fe_{0.5}Co_{0.5}OOH$ with Fe^{3+}-O-Fe^{3+} motifs for oxygen evolution reaction. Appl Catal B-Environ 304:120986. https://doi.org/10.1016/j.apcatb.2021.120986
16. Niu S, Jiang WJ, Wei Z, Tang T, Ma J, Hu JS, Wan LJ (2019) Se-doping activates FeOOH for cost-effective and efficient electrochemical water oxidation. J Am Chem Soc 141(17):7005–7013. https://doi.org/10.1021/jacs.9b01214
17. Zhang X, Zhao Y, Zhao Y, Shi R, Waterhouse GI, Zhang T (2019) A simple synthetic strategy toward defect-rich porous monolayer NiFe-layered double hydroxide nanosheets for efficient electrocatalytic water oxidation. Adv Energy Mater 9(24):1900881. https://doi.org/10.1002/aenm.201900881
18. Jiang J, Sun F, Zhou S, Hu W, Zhang H, Dong J, Jiang Z, Zhao J, Li J, Yan W, Wang M (2018) Atomic-level insight into super-efficient electrocatalytic oxygen evolution on iron and vanadium co-doped nickel (oxy) hydroxide. Nat Commun 9(1):1–12. https://doi.org/10.1038/s41467-018-05341-y
19. Yang Y, Zhang K, Lin H, Li X, Chan HC, Yang L, Gao Q (2017) MoS_2-Ni_3S_2 heteronanorods as efficient and stable bifunctional electrocatalysts for overall water splitting. ACS Catal 7(4):2357–2366. https://doi.org/10.1021/acscatal.6b03192
20. Guo HP, Ruan BY, Luo WB, Deng J, Wang JZ, Liu HK, Dou SX (2018) Ultrathin and edge-enriched holey nitride nanosheets as bifunctional electrocatalysts for the oxygen and hydrogen evolution reactions. ACS Catal 8(10):9686–9696. https://doi.org/10.1021/acscatal.8b01821
21. Radwan A, Jin H, He D, Mu S (2021) Design engineering, synthesis protocols, and energy applications of MOF-derived electrocatalysts. Nano-Micro Lett 13(1):1–32. https://doi.org/10.1007/s40820-021-00656-w
22. Sun H, Ma Z, Qiu Y, Liu H, Gao GG (2018) Ni@ NiO nanowires on nickel foam prepared via "acid hungry" strategy: high supercapacitor performance and robust electrocatalysts for water splitting reaction. Small 14(31):1800294. https://doi.org/10.1002/smll.201800294
23. Liang C, Zou P, Nairan A, Zhang Y, Liu J, Liu K, Hu S, Kang F, Fan JH, Yang C (2020) Exceptional performance of hierarchical Ni-Fe oxyhydroxide@ NiFe alloy nanowire array electrocatalysts for large current density water splitting. Energy Environ Sci 13(1):86–95. https://doi.org/10.1039/c9ee02388g
24. Tang YJ, Wang Y, Wang XL, Li SL, Huang W, Dong LZ, Liu CH, Li YF, Lan YQ (2016) Molybdenum disulfide/nitrogen-doped reduced graphene oxide nanocomposite with enlarged interlayer spacing for electrocatalytic hydrogen evolution. Adv Energy Mater 6(12):1600116. https://doi.org/10.1002/aenm.201600116
25. Guan C, Xiao W, Wu H, Liu X, Zang W, Zhang H, Ding J, Feng YP, Pennycook SJ, Wang J (2018) Hollow Mo-doped CoP nanoarrays for efficient overall water splitting. Nano Energy 48:73–80. https://doi.org/10.1016/j.nanoen.2018.03.034
26. Peng S, Gong F, Li L, Yu D, Ji D, Zhang T, Hu Z, Zhang Z, Chou S, Du Y, Ramakrishna S (2018) Necklace-like multishelled hollow spinel oxides with oxygen vacancies for efficient water electrolysis. J Am Chem Soc 140(42):13644–13653. https://doi.org/10.1021/jacs.8b05134
27. Man IC, Su HY, Calle-Vallejo F, Hansen HA, Martínez JI, Inoglu NG, Kitchin J, Jaramillo TF, Nørskov JK, Rossmeisl J (2011) Universality in oxygen evolution electrocatalysis on oxide surfaces. ChemCatChem 3(7):1159–1165. https://doi.org/10.1002/cctc.201000397
28. Suntivich J, May KJ, Gasteiger HA, Goodenough JB, Shao-Horn Y (2011) A perovskite oxide optimized for oxygen evolution catalysis from molecular orbital principles. Science 334(6061):1383–1385. https://doi.org/10.1126/science.1212858
29. Xu K, Ding H, Lv HF, Chen PZ, Lu XL, Cheng H, Zhou TP, Liu S, Wu XJ, Wu CZ, Xie Y (2016) Dual electrical-behavior regulation on electrocatalysts realizing enhanced electrochemical water oxidation. Adv Mater 28(17):3326–3332. https://doi.org/10.1002/adma.201505732
30. Huang JH, Chen JT, Yao T, He JF, Jiang S, Sun ZH, Liu QH, Cheng WR, Hu FC, Jiang Y, Pan ZY, Wei SQ (2015) CoOOH nanosheets with high mass activity for water oxidation. Angew Chem 127(30):8846–8851. https://doi.org/10.1002/ange.201502836
31. Xia C, Jiang Q, Zhao C, Hedhili MN, Alshareef HN (2016) Selenide-based electrocatalysts and scaffolds for water oxidation applications. Adv Mater 28(1):77–85. https://doi.org/10.1002/adma.201503906
32. Stevens MB, Enman LJ, Batchellor AS, Cosby MR, Vise AE, Trang CDM, Boettcher SW (2017) Measurement techniques for the study of thin film heterogeneous water oxidation electrocatalysts. Chem Mater 29(1):120–140. https://doi.org/10.1021/acs.chemmater.6b02796
33. Trotochaud L, Young SL, Ranney JK, Boettcher SW (2014) Nickel-iron oxyhydroxide oxygen-evolution electrocatalysts: the role of intentional and incidental iron incorporation. J Am Chem Soc 136(18):6744–6753. https://doi.org/10.1021/ja502379c
34. Matsumoto Y, Sato E (1986) Electrocatalytic properties of transition metal oxides for oxygen evolution reaction. Mater Chem Phys 14(5):397–426. https://doi.org/10.1016/0254-0584(86)90045-3
35. Sun M, Lu Z, Luo L, Chang Z, Sun X (2016) A 3D porous Ni-Cu alloy film for high-performance hydrazine electrooxidation. Nanoscale 8(3):1479–1484. https://doi.org/10.1039/C5NR07072D
36. Xu W, Lu Z, Wan P, Kuang Y, Sun X (2016) High-performance water electrolysis system with double nanostructured superaerophobic electrodes. Small 12(18):2492–2498. https://doi.org/10.1002/smll.201600189
37. Yu M, Zheng J, Guo M (2022) La-doped NiFe-LDH coupled with hierarchical vertically aligned MXene frameworks for efficient overall water splitting. J Energy Chem 70:472–479. https://doi.org/10.1016/j.jechem.2022.02.044
38. Chen X, Wu Y, Su B, Wang J, Song Y, Jiang L (2012) Terminating marine methane bubbles by superhydrophobic sponges. Adv Mater 24(43):5884–5889. https://doi.org/10.1002/adma.201202061
39. Nixon E, Pantoya ML, Sivakumar G, Vijayasai A, Dallas T (2011) Effect of a superhydrophobic coating on the combustion of aluminium and iron oxide nanothermites. Surf Coat Technol 205(21–22):5103–5108. https://doi.org/10.1016/j.surfcoat.2011.05.014
40. Darband GB, Aliofkhazraei M, Shanmugam S (2019) Recent advances in methods and technologies for enhancing bubble detachment during electrochemical water splitting. Renew Sustain Energy Rev 114:109300. https://doi.org/10.1016/j.rser.2019.109300
41. Zhao K, Yang W, Li L, Wang S, Wang L, Qi Z, Yang Y, Chen Z, Zhuang J, Hao J, Shi W (2022) Discharge induced-activation of phosphorus-doped nickel oxyhydroxide for oxygen evolution reaction. Chem Eng J 435:135049. https://doi.org/10.1016/j.cej.2022.135049
42. Wu YJ, Yang J, Tu TX, Li WQ, Zhang P, Zhou Y, Li JF, Li JT, Sun SG (2021) Evolution of cationic vacancy defects: a motif for surface restructuration of OER precatalyst. Angew Chem Int Ed 60(51):26829–26836. https://doi.org/10.1002/anie.202112447

43. Liu H, He Q, Jiang H, Lin Y, Zhang Y, Habib M, Chen S, Song L (2017) Electronic structure reconfiguration toward pyrite NiS_2 via engineered heteroatom defect boosting overall water splitting. ACS Nano 11(11):11574–11583. https://doi.org/10.1021/acsnano.7b06501
44. Peng L, Yang N, Yang Y, Wang Q, Xie X, Sun-Waterhouse D, Shang L, Zhang T, Waterhouse GIN (2021) Atomic cation-vacancy engineering of NiFe-layered double hydroxides for improved activity and stability towards the oxygen evolution reaction. Angew Chem Int Ed 133(46):24817–24824. https://doi.org/10.1002/ange.202109938
45. Yu J, Le TA, Tran NQ, Lee H (2020) Earth-abundant transition-metal-based bifunctional electrocatalysts for overall water splitting in alkaline media. Chem A Eur J 26(29):6423–6436. https://doi.org/10.1002/chem.202000209
46. Wu M, Liu Y, Zhu Y, Lin J, Liu J, Hu H, Wang Y, Zhao Q, Lv R, Qiu J (2017) Supramolecular polymerization-assisted synthesis of nitrogen and sulfur dual-doped porous graphene networks from petroleum coke as efficient metal-free electrocatalysts for the oxygen reduction reaction. J Mater Chem A 5(22):11331–11339. https://doi.org/10.1039/C7TA03264A
47. Ding X, Huang H, Wan Q, Guo X, Fang Y, Lin S, Chen D, Xie Z (2021) Self-template synthesis of hollow Fe-doped CoP prisms with enhanced oxygen evolution reaction activity. J Energy Chem 62:415–422. https://doi.org/10.1016/j.jechem.2021.04.001
48. Han P, Tan T, Wu F, Cai P, Cheng G, Luo W (2020) Nickel-iron borate coated nickel-iron boride hybrid for highly stable and active oxygen evolution electrocatalysis. Chinese Chem Lett 31(9):2469–2472. https://doi.org/10.1016/j.cclet.2020.03.009
49. Li S, Liu Z, Wang F, Yuan NY (2021) Ce-Doped FeNi-layered double hydroxide nanosheets grown on an open-framework nickel phosphate nanorod array for oxygen evolution reaction. ACS Appl Energy Mater 4(11):12836–12847. https://doi.org/10.1021/acsaem.1c02531
50. Tüysüz H, Hwang YJ, Khan SB, Asiri AM, Yang P (2013) Mesoporous Co_3O_4 as an electrocatalyst for water oxidation. Nano Res 6(1):47–54. https://doi.org/10.1007/s12274-012-0280-8
51. Li X, Wang C, Liu YY, Xue H, Pang H, Xu Q (2021) Cu-alanine complex-derived CuO electrocatalysts with hierarchical nanostructures for efficient oxygen evolution. Chin Chem Lett 32(7):2239–2242. https://doi.org/10.1016/j.cclet.2020.12.037
52. Grzelczak M, Zhang J, Pfrommer J, Hartmann J, Driess M, Antonietti M, Wang X (2013) Electro- and photochemical water oxidation on ligand-free Co_3O_4 nanoparticles with tunable sizes. ACS Catal 3(3):383–388. https://doi.org/10.1021/cs3007523
53. Yan D, Li Y, Huo J, Chen R, Dai L, Wang S (2017) Defect chemistry of nonprecious-metal electrocatalysts for oxygen reactions. Adv Mater 29(48):1606459. https://doi.org/10.1002/adma.201606459
54. Yu XY, Lou XW (2018) Mixed metal sulfides for electrochemical energy storage and conversion. Adv Energy Mater 8(3):1701592. https://doi.org/10.1002/aenm.201701592
55. Li M, Liu Z, Zha Q, Li S, Ni Y (2021) Non-precious metal nanotube arrays hybrid catalyst prepared by a mutual template method for efficient water oxidation in alkaline medium. Chem Eng J 410:128330. https://doi.org/10.1016/j.cej.2020.128330
56. Li D, Li X, Hou X, Sun X, Liu B, He D (2014) Building a Ni_3S_2 nanotube array and investigating its application as an electrode for lithium ion batteries. Chem Commun 50(66):9361–9364. https://doi.org/10.1039/C4CC01311E
57. Qi J, Lin YP, Chen D, Zhou T, Zhang W, Cao R (2020) Autologous cobalt phosphates with modulated coordination sites for electrocatalytic water oxidation[J]. Angew Chem 132(23):9002–9006. https://doi.org/10.1002/ange.202001737
58. Chen S, Chen B, Wang S, Yan W, He Y, Guo Z, Xu R (2020) Ag doping to boost the electrochemical performance and corrosion resistance of Ti/Sn-Sb-RuOx/α-PbO_2/β-PbO_2 electrode in zinc electrowinning. J Alloy Compd 815:152551. https://doi.org/10.1016/j.jallcom.2019.152551
59. Yuan LP, Tang T, Hu JS, Wan LJ (2021) Confinement strategies for precise synthesis of efficient electrocatalysts from the macroscopic to the atomic level. Acc Mater Res 2(10):907–919. https://doi.org/10.1021/accountsmr.1c00135
60. Liang Y, Li Y, Wang H, Zhou J, Wang J, Regier T, Dai H (2011) Co_3O_4 nanocrystals on graphene as a synergistic catalyst for oxygen reduction reaction. Nat Mater 10(10):780–786. https://doi.org/10.1038/nmat3087
61. Xu L, Jiang Q, Xiao Z, Li X, Huo J, Wang S, Dai L (2016) Plasma-engraved Co_3O_4 nanosheets with oxygen vacancies and high surface area for the oxygen evolution reaction. Angew Chem 128(17):5363–5367. https://doi.org/10.1002/ange.201600687
62. Cai Z, Bi Y, Hu E, Liu W, Dwarica N, Tian Y, Li X, Kuang Y, Li Y, Yang XQ, Wang X, Sun X (2018) Single-crystalline ultrathin Co_3O_4 nanosheets with massive vacancy defects for enhanced electrocatalysis. Adv Energy Mater 8(3):1701694. https://doi.org/10.1002/aenm.201701694
63. Babar PT, Lokhande AC, Gang MG, Pawar BS, Pawar SM, Kim JH (2018) Thermally oxidized porous NiO as an efficient oxygen evolution reaction (OER) electrocatalyst for electrochemical water splitting application. J Ind Eng Chem 60:493–497. https://doi.org/10.1016/j.jiec.2017.11.037
64. Ji X, Ma M, Ge R, Ren X, Wang H, Liu J, Liu Z, Asiri AM, Sun X (2017) WO_3 nanoarray: an efficient electrochemical oxygen evolution catalyst electrode operating in alkaline solution. Inorg Chem 56(24):14743–14746. https://doi.org/10.1021/acs.inorgchem.7b02552
65. Liu G, Karuturi SK, Chen H, Wang D, Ager JW, Simonov AN, Tricoli A (2020) Enhancement of the photoelectrochemical water splitting by perovskite $BiFeO_3$ via interfacial engineering. Sol Energy 202:198–203. https://doi.org/10.1016/j.solener.2020.03.117
66. Lu XF, Gu LF, Wang JW, Wu JX, Liao PQ, Li GR (2017) Bimetal-organic framework derived $CoFe_2O_4$/C porous hybrid nanorod arrays as high-performance electrocatalysts for oxygen evolution reaction. Adv Mater 29(3):1604437. https://doi.org/10.1002/adma.201604437
67. Gao C, Wang J, Ma K, Lu Y, Zhao Z (2021) Efficient oxygen evolution catalysts with synergistic reactivity: $CoFe_2O_4$/C derived from bimetallic organic framework supported on nitrogen-doped carbon nanoarray structure. Mater Res Bull 139:111287. https://doi.org/10.1016/j.materresbull.2021.111287
68. Ling X, Du F, Zhang Y, Shen Y, Li T, Alsaedi A, Hayat T, Zhou Y, Zou Z (2019) Preparation of an Fe_2Ni MOF on nickel foam as an efficient and stable electrocatalyst for the oxygen evolution reaction. RSC Adv 9(57):33558–33562. https://doi.org/10.1039/C9RA07499F
69. Zhao L, Dong B, Li S et al (2017) Interdiffusion reaction-assisted hybridization of two-dimensional metal-organic frameworks and $Ti_3C_2T_x$ nanosheets for electrocatalytic oxygen evolution. ACS Nano 11(6):5800–5807. https://doi.org/10.1021/acsnano.7b01409
70. Li FL, Shao Q, Huang X, Lang JP (2018) Nanoscale trimetallic metal-organic frameworks enable efficient oxygen evolution electrocatalysis. Angew Chem 130(7):1906–1910. https://doi.org/10.1002/ange.201711376
71. Yuan JT, Hou JJ, Liu XL, Feng YR, Zhang XM (2020) Optimized trimetallic benzotriazole-5-carboxylate MOFs with coordinately unsaturated active sites as an efficient electrocatalyst for the oxygen evolution reaction. Dalton Trans 49(3):750–756. https://doi.org/10.1039/C9DT04295D

72. Zhao S, Wang Y, Dong J et al (2016) Ultrathin metal-organic framework nanosheets for electrocatalytic oxygen evolution. Nat Energy 1(12):1–10. https://doi.org/10.1038/nenergy.2016.184
73. Rui K, Zhao G, Chen Y, Lin Y, Zhou Q, Chen J, Zhu J, Sun W, Huang W, Dou SX (2018) Hybrid 2D dual-metal-organic frameworks for enhanced water oxidation catalysis. Adv Func Mater 28(26):1801554. https://doi.org/10.1002/adfm.201801554
74. Chen P, Xu K, Fang Z, Tong Y, Wu J, Lu X, Peng X, Ding H, Wu C, Xie Y (2015) Metallic Co_4N porous nanowire arrays activated by surface oxidation as electrocatalysts for the oxygen evolution reaction. Angew Chem 127(49):14923–14927. https://doi.org/10.1002/ange.201506480
75. Jia J, Zhai M, Lv J, Zhao B, Du H, Zhu J (2018) Nickel molybdenum nitride nanorods grown on Ni foam as efficient and stable bifunctional electrocatalysts for overall water splitting. ACS Appl Mater Interfaces 10(36):30400–30408. https://doi.org/10.1021/acsami.8b09854
76. Wang Y, Zhang B, Pan W, Ma H, Zhang J (2017) 3D porous nickel–cobalt nitrides supported on nickel foam as efficient electrocatalysts for overall water splitting. Chemsuschem 10(21):4170–4177. https://doi.org/10.1002/cssc.201701456
77. Wang Y, Liu D, Liu Z, Xie C, Huo J, Wang S (2016) Porous cobalt-iron nitride nanowires as excellent bifunctional electrocatalysts for overall water splitting. Chem Commun 52(85):12614–12617. https://doi.org/10.1039/C6CC06608A
78. Zhu C, Yin Z, Lai W, Sun Y, Liu L, Zhang X, Chen Y, Chou SL (2018) Fe-Ni-Mo nitride porous nanotubes for full water splitting and Zn-air batteries. Adv Energy Mater 8(36):1802327. https://doi.org/10.1002/aenm.201802327
79. Liu SQ, Gao MR, Liu S, Luo JL (2021) Hierarchically assembling cobalt/nickel carbonate hydroxide on copper nitride nanowires for highly efficient water splitting. Appl Catal B 292:120148. https://doi.org/10.1016/j.apcatb.2021.120148
80. Lin J, Wang P, Wang H, Li C, Si X, Qi J, Cao J, Zhong Z, Fei W, Feng J (2019) Defect-rich heterogeneous MoS_2/NiS_2 nanosheets electrocatalysts for efficient overall water splitting. Adv Sci 6(14):1900246. https://doi.org/10.1002/advs.201900246
81. Wang B, Tang C, Wang HF, Li BQ, Cui X, Zhang Q (2018) Anion-regulated hydroxysulfide monoliths as OER/ORR/HER electrocatalysts and their applications in self-powered electrochemical water splitting. Small Methods 2(12):1800055. https://doi.org/10.1002/smtd.201800055
82. Lu X, Zhao C (2015) Electrodeposition of hierarchically structured three-dimensional nickel–iron electrodes for efficient oxygen evolution at high current densities. Nat Commun 6(1):1–7. https://doi.org/10.1038/ncomms7616
83. Tang C, Wang HS, Wang HF, Zhang Q, Tian GL, Nie JQ, Wei F (2015) Spatially confined hybridization of nanometer-sized NiFe hydroxides into nitrogen-doped graphene frameworks leading to superior oxygen evolution reactivity[J]. Adv Mater 27(30):4516–4522. https://doi.org/10.1002/adma.201501901
84. Wang J, Cui W, Liu Q, Xing Z, Asiri AM, Sun X (2016) Recent progress in cobalt-based heterogeneous catalysts for electrochemical water splitting. Adv Mater 28(2):215–230. https://doi.org/10.1002/adma.201502696
85. Wang F, Liu Z, Zhang K et al (2021) Ce-Doped Ni–S nanosheets on Ni foam supported $NiMoO_4$ micropillars: fast electrodeposition, improved electrocatalytic activity and ultralong durability for the oxygen evolution reaction in various electrolytes[J]. Dalton Trans 50(47):17774–17784. https://doi.org/10.1039/D1DT03266F
86. Xiao Z, Wang Y, Huang YC, Wei Z, Dong CL, Ma J, Shen S, Li Y, Wang S (2017) Filling the oxygen vacancies in Co_3O_4 with phosphorus: an ultra-efficient electrocatalyst for overall water splitting. Energy Environ Sci 10(12):2563–2569. https://doi.org/10.1039/C7EE01917C
87. Zhao Y, Chang C, Teng F, Zhao Y, Chen G, Shi R, Waterhouse GIN, Huang W, Zhang T (2017) Defect-engineered ultrathin δ-MnO_2 nanosheet arrays as bifunctional electrodes for efficient overall water splitting. Adv Energy Mater 7(18):1700005. https://doi.org/10.1002/aenm.201700005
88. Zhuang L, Ge L, Yang Y, Li M, Jia Y, Yao X, Zhu Z (2017) Ultrathin iron-cobalt oxide nanosheets with abundant oxygen vacancies for the oxygen evolution reaction. Adv Mater 29(17):1606793. https://doi.org/10.1002/adma.201606793
89. Ling T, Zhang T, Ge B, Han L, Zheng L, Lin F, Xu Z, Hu WB, Du XW, Davey K, Qiao SZ (2019) Well-dispersed nickel- and zinc-tailored electronic structure of a transition metal oxide for highly active alkaline hydrogen evolution reaction. Adv Mater 31(16):1807771. https://doi.org/10.1002/adma.201807771
90. Zhou Y, Sun S, Song J, Xi S, Chen B, Du Y, Fisher AC, Cheng F, Wang X, Zhang H, Xu ZJ (2018) Enlarged Co-O covalency in octahedral sites leading to highly efficient spinel oxides for oxygen evolution reaction. Adv Mater 30(32):1802912. https://doi.org/10.1002/adma.201802912
91. Yagi S, Yamada I, Tsukasaki H, Seno A, Murakami M, Fujii H, Chen H, Umezawa N, Abe H, Nishiyama N, Mori S (2015) Covalency-reinforced oxygen evolution reaction catalyst. Nat Commun 6(1):1–6. https://doi.org/10.1038/ncomms9249
92. Liu G, Chen H, Xia L, Wang S, Ding LX, Li D, Xiao K, Dai S, Wang H (2015) Hierarchical mesoporous/macroporous perovskite $La_{0.5}Sr_{0.5}CoO_{3-x}$ nanotubes: a bifunctional catalyst with enhanced activity and cycle stability for rechargeable lithium oxygen batteries. ACS Appl Mater Interfaces 7(40):22478–22486. https://doi.org/10.1021/acsami.5b06587
93. Zhu Y, Lin Q, Wang Z, Qi Z, Yin D, Liu Y, Zhang X, Shao Z, Wang H (2021) Chlorine-anion doping induced multi-factor optimization in perovskites for boosting intrinsic oxygen evolution. J Energy Chem 52:115–120. https://doi.org/10.1016/j.jechem.2020.03.055
94. Wang HF, Chen L, Pang H, Kaskel S, Xu Q (2020) MOF-derived electrocatalysts for oxygen reduction, oxygen evolution and hydrogen evolution reactions. Chem Soc Rev 49(5):1414–1448. https://doi.org/10.1039/C9CS00906J
95. Ding M, Flaig RW, Jiang HL, Yaghi OM (2019) Carbon capture and conversion using metal-organic frameworks and MOF-based materials. Chem Soc Rev 48(10):2783–2828. https://doi.org/10.1039/C8CS00829A
96. Zha Q, Li M, Liu Z, Ni Y (2020) Hierarchical Co, Fe-MOF-74/Co/carbon cloth hybrid electrode: simple construction and enhanced catalytic performance in full water splitting. ACS Sustain Chem Eng 8(32):12025–12035. https://doi.org/10.1021/acssuschemeng.0c02993
97. Zha Q, Yuan F, Qin G, Ni Y (2020) Cobalt-based MOF-on-MOF two-dimensional heterojunction nanostructures for enhanced oxygen evolution reaction electrocatalytic activity. Inorg Chem 59(2):1295–1305. https://doi.org/10.1021/acs.inorgchem.9b03011
98. Zhang W, Wang Y, Zheng H, Li R, Tang Y, Li B, Zhu C, You L, Gao MR, Liu Z, Yu SH, Zhou K (2020) Embedding ultrafine metal oxide nanoparticles in monolayered metal–organic framework nanosheets enables efficient electrocatalytic oxygen evolution. ACS Nano 14(2):1971–1981. https://doi.org/10.1021/acsnano.9b08458
99. Huang H, Zhao Y, Bai Y, Li F, Zhang Y, Chen Y (2020) Conductive metal-organic frameworks with extra metallic sites as an efficient electrocatalyst for the hydrogen evolution reaction. Adv Sci 7(9):2000012. https://doi.org/10.1002/advs.202000012
100. Xue Z, Liu K, Liu Q, Li Y, Li M, Su CY, Ogiwara N, Kobayashi H, Kitagawa H, Liu M, Li G (2019) Missing-linker metal-organic

frameworks for oxygen evolution reaction. Nat Commun 10(1):1–8. https://doi.org/10.1038/s41467-019-13051-2
101. Wan K, Luo J, Zhang X, Subramanian P, Fransaer J (2021) Sulfur-modified nickel selenide as an efficient electrocatalyst for the oxygen evolution reaction. J Energy Chem 62:198–203. https://doi.org/10.1016/j.jechem.2021.03.013
102. Yang HB, Miao J, Hung SF et al (2016) Identification of catalytic sites for oxygen reduction and oxygen evolution in N-doped graphene materials: development of highly efficient metal-free bifunctional electrocatalyst. Sci Adv 2(4):e1501122. https://doi.org/10.1126/sciadv.1501122
103. Shen JQ, Liao PQ, Zhou DD, He CT, Wu JX, Zhang WX, Zhang JP, Chen XM (2017) Modular and stepwise synthesis of a hybrid metal-organic framework for efficient electrocatalytic oxygen evolution. J Am Chem Soc 139(5):1778–1781. https://doi.org/10.1021/jacs.6b12353
104. Lu XF, Liao PQ, Wang JW, Wu JX, Chen XW, He CT, Zhang JP, Li GR, Chen XM (2016) An alkaline-stable, metal hydroxide mimicking metal-organic framework for efficient electrocatalytic oxygen evolution. J Am Chem Soc 138(27):8336–8339. https://doi.org/10.1021/jacs.6b03125
105. Wang Q, Astruc D (2019) State of the art and prospects in metal–organic framework (MOF)-based and MOF-derived nanocatalysis. Chem Rev 120(2):1438–1511. https://doi.org/10.1021/acs.chemrev.9b00223
106. Cheng W, Wu ZP, Luan D, Zang SQ, Lou (David) XW, (2021) Synergetic cobalt-copper-based bimetal–organic framework nanoboxes toward efficient electrochemical oxygen evolution. Angew Chem Int Ed 60(50):26397–26402. https://doi.org/10.1002/anie.202112775
107. Chen Y, Huang N, Liang Y (2021) Preparation of CeO_2/Cu-MOF/GO composite for efficient electrocatalytic oxygen evolution reaction. Ionics 27(10):4347–4360
108. Jahan M, Liu Z, Loh KP (2013) A graphene oxide and copper-centered metal organic framework composite as a tri-functional catalyst for HER, OER, and ORR. Adv Func Mater 23(43):5363–5372. https://doi.org/10.1002/adfm.201300510
109. Chen P, Li N, Chen X, Ong WJ, Zhao X (2017) The rising star of 2D black phosphorus beyond graphene: synthesis, properties and electronic applications. 2D Mater 5(1):014002. https://doi.org/10.1088/2053-1583/aa8d37
110. Sinha ASK, Ojha U (2021) Recent trends in development of metal nitride nanocatalysts for water electrolysis application. In Electrocatalysis; IntechOpen: London, UK. https://doi.org/10.5772/intechopen.95748
111. Zhang Y, Ouyang B, Xu J, Jia G, Chen S, Rawat RS, Fan HJ (2016) Rapid synthesis of cobalt nitride nanowires: highly efficient and low-cost catalysts for oxygen evolution. Angew Chem 128(30):8812–8816. https://doi.org/10.1002/ange.201604372
112. Shalom M, Molinari V, Esposito D, Clavel G, Ressnig D, Giordano C, Antonietti M (2014) Sponge-like nickel and nickel nitride structures for catalytic applications. Adv Mater 26(8):1272–1276. https://doi.org/10.1002/adma.201304288
113. Ma L, Ting LRL, Molinari V, Giordano C, Yeo BS (2015) Efficient hydrogen evolution reaction catalyzed by molybdenum carbide and molybdenum nitride nanocatalysts synthesized via the urea glass route. J Mater Chem A 3(16):8361–8368. https://doi.org/10.1039/C5TA00139K
114. Zhang J, Wang T, Pohl D, Rellinghaus B, Dong R, Liu S, Zhang X, Feng X (2016) Interface engineering of MoS_2/Ni_3S_2 heterostructures for highly enhanced electrochemical overall-water-splitting activity. Angew Chem 128(23):6814–6819. https://doi.org/10.1002/ange.201602237
115. Guan C, Liu X, Elshahawy AM, Zhang H, Wu H, Pennycook SJ, Wang J (2017) Metal-organic framework derived hollow CoS_2 nanotube arrays: an efficient bifunctional electrocatalyst for overall water splitting. Nanoscale Horiz 2(6):342–348. https://doi.org/10.1039/C7NH00079K
116. Duan J, Chen S, Vasileff A, Qiao SZ (2016) Anion and cation modulation in metal compounds for bifunctional overall water splitting. ACS Nano 10(9):8738–8745. https://doi.org/10.1021/acsnano.6b04252
117. Wang B, Tang C, Wang HF, Chen X, Cao R, Zhang Q (2019) A nanosized CoNi hydroxide@ hydroxysulfide core-shell heterostructure for enhanced oxygen evolution. Adv Mater 31(4):1805658. https://doi.org/10.1002/adma.201805658
118. Xue Z, Li X, Liu Q, Cai M, Liu K, Liu M, Ke Z, Liu X, Li G (2019) Interfacial electronic structure modulation of NiTe nanoarrays with NiS nanodots facilitates electrocatalytic oxygen evolution. Adv Mater 31(21):1900430. https://doi.org/10.1002/adma.201900430
119. Nørskov JK, Bligaard T, Rossmeisl J, Christensen CH (2009) Towards the computational design of solid catalysts. Nat Chem 1(1):37–46. https://doi.org/10.1038/nchem.121
120. Cui L, Zhang W, Zheng R, Liu J (2020) Electrocatalysts based on transition metal borides and borates for the oxygen evolution reaction. Chem A Eur J 26(51):11661–11672. https://doi.org/10.1002/chem.202000880
121. Zhang B, Zheng Y, Ma T, Yang C, Peng Y, Zhou Z, Zhou M, Li S, Wang Y, Cheng C (2021) Designing MOF nanoarchitectures for electrochemical water splitting. Adv Mater 33(17):2006042. https://doi.org/10.1002/adma.202006042
122. Zhao CX, Li BQ, Zhao M, Liu JN, Zhao LD, Chen X, Zhang Q (2020) Precise anionic regulation of NiFe hydroxysulfide assisted by electrochemical reactions for efficient electrocatalysis. Energ Environ Sci 13(6):1711–1716. https://doi.org/10.1039/C9EE03573G
123. Yuan F, Zhang E, Liu Z, Yang K, Zha Q, Ni Y (2021) Hollow CoS_x nanoparticles grown on FeCo-LDH microtubes for enhanced electrocatalytic performances for the oxygen evolution reaction. ACS Appl Energ Mater 4(11):12211–12223. https://doi.org/10.1021/acsaem.1c01947
124. Yang R, Zhou Y, Xing Y, Li D, Jiang D, Chen M, Shi W, Yuan S (2019) Synergistic coupling of CoFe-LDH arrays with NiFe-LDH nanosheet for highly efficient overall water splitting in alkaline media. Appl Catal B 253:131–139. https://doi.org/10.1016/j.apcatb.2019.04.054
125. Dong Y, Komarneni S (2021) Strategies to develop earth-abundant heterogeneous oxygen evolution reaction catalysts for pH-neutral or pH-near-neutral electrolytes. Small Methods 5(1):2000719. https://doi.org/10.1002/smtd.202000719
126. Fan K, Li Z, Song Y, Xie W, Shao M, Wei M (2021) Confinement synthesis based on layered double hydroxides: a new strategy to construct single-atom-containing integrated electrodes. Adv Func Mater 31(10):2008064. https://doi.org/10.1002/adfm.202008064
127. Yuan F, Wei J, Qin G, Ni Y (2020) Carbon cloth supported hierarchical core-shell NiCo2S4@ CoNi-LDH nanoarrays as catalysts for efficient oxygen evolution reaction in alkaline solution. J Alloy Compd 830:154658. https://doi.org/10.1016/j.jallcom.2020.154658
128. Wang D, Zhou J, Hu Y, Yang J, Han N, Li Y, Sham TK (2015) In situ X-ray absorption near-edge structure study of advanced $NiFe(OH)_x$ electrocatalyst on carbon paper for water oxidation. J Phys Chem C 119(34):19573–19583. https://doi.org/10.1021/acs.jpcc.5b02685
129. Friebel D, Louie MW, Bajdich M et al (2015) Identification of highly active Fe sites in (Ni, Fe)OOH for electrocatalytic water splitting. J Am Chem Soc 137(3):1305–1313. https://doi.org/10.1021/ja511559d
130. Zhang H, Li X, Hähnel A, Naumann V, Lin C, Azimi S, Schweizer SL, Maijenburg AW, Wehrspohn RB (2018) Bifunctional

heterostructure assembly of NiFe LDH nanosheets on NiCoP nanowires for highly efficient and stable overall water splitting. Adv Func Mater 28(14):1706847. https://doi.org/10.1002/adfm.201706847
131. Zhang Y, Xie W, Ma J, Chen L, Chen C, Zhang X, Shao M (2021) Active facet determination of layered double hydroxide for oxygen evolution reaction. J Energy Chem 60:127–134. https://doi.org/10.1016/j.jechem.2020.12.038
132. Cantor B, Chang ITH, Knight P, Vincent AJB (2004) Microstructural development in equiatomic multicomponent alloys. Mater Sci Eng, A 375:213–218. https://doi.org/10.1016/j.msea.2003.10.257
133. Yeh JW, Chen SK, Lin SJ, Gan JY, Chin TS, Shun TT, Tsau CH, Chang SY (2004) Nanostructured high-entropy alloys with multiple principal elements: novel alloy design concepts and outcomes. Adv Eng Mater 6(5):299–303. https://doi.org/10.1002/adem.200300567
134. Miracle DB, Senkov ON (2017) A critical review of high entropy alloys and related concepts. Acta Mater 122:448–511. https://doi.org/10.1016/j.actamat.2016.08.081
135. Lu Y, Gao X, Jiang L et al (2017) Directly cast bulk eutectic and near-eutectic high entropy alloys with balanced strength and ductility in a wide temperature range. Acta Mater 124:143–150. https://doi.org/10.1016/j.actamat.2016.11.016
136. Lu C, Niu L, Chen N et al (2016) Enhancing radiation tolerance by controlling defect mobility and migration pathways in multicomponent single-phase alloys. Nat Commun 7(1):1–8. https://doi.org/10.1038/ncomms13564
137. Liu H, Syama L, Zhang L, Lee C, Liu C, Dai Z, Yan Q (2021) High-entropy alloys and compounds for electrocatalytic energy conversion applications. SusMat 1(4):482–505. https://doi.org/10.1002/sus2.32
138. Zhang Y, Wang D, Wang S (2022) High-entropy alloys for electrocatalysis: design, characterization, and applications. Small 18(7):2104339. https://doi.org/10.1002/smll.202104339
139. Cui X, Zhang B, Zeng C, Guo S (2018) Electrocatalytic activity of high-entropy alloys toward oxygen evolution reaction. MRS Commun 8(3):1230–1235. https://doi.org/10.1557/mrc.2018.111
140. Qiu HJ, Fang G, Gao J, Wen Y, Lv J, Li H, Xue G, Liu X, Sun S (2019) Noble metal-free nanoporous high-entropy alloys as highly efficient electrocatalysts for oxygen evolution reaction. ACS Mater Lett 1(5):526–533. https://doi.org/10.1021/acsmaterialslett.9b00414
141. Dai W, Lu T, Pan Y (2019) Novel and promising electrocatalyst for oxygen evolution reaction based on MnFeCoNi high entropy alloy. J Power Sources 430:104–111. https://doi.org/10.1016/j.jpowsour.2019.05.030
142. Sun Y, Dai S (2021) High-entropy materials for catalysis: a new frontier. Sci Adv 7(20):eabg1600. https://doi.org/10.1126/sciadv.abg1600
143. Ding Z, Bian J, Shuang S, Liu X, Hu Y, Sun C, Yang Y (2020) High entropy intermetallic–oxide core–shell nanostructure as superb oxygen evolution reaction catalyst. Adv Sustain Syst 4(5):1900105. https://doi.org/10.1002/adsu.201900105
144. Yao Y, Liu Z, Xie P et al (2020) Computationally aided, entropy-driven synthesis of highly efficient and durable multi-elemental alloy catalysts. Sci Adv 6(11):eaaz0510. https://doi.org/10.1126/sciadv.aaz0510
145. Zhang L, Cai W, Bao N (2021) Top-level design strategy to construct an advanced high-entropy Co-Cu-Fe-Mo (oxy) hydroxide electrocatalyst for the oxygen evolution reaction. Adv Mater 33(22):2100745. https://doi.org/10.1002/adma.202100745